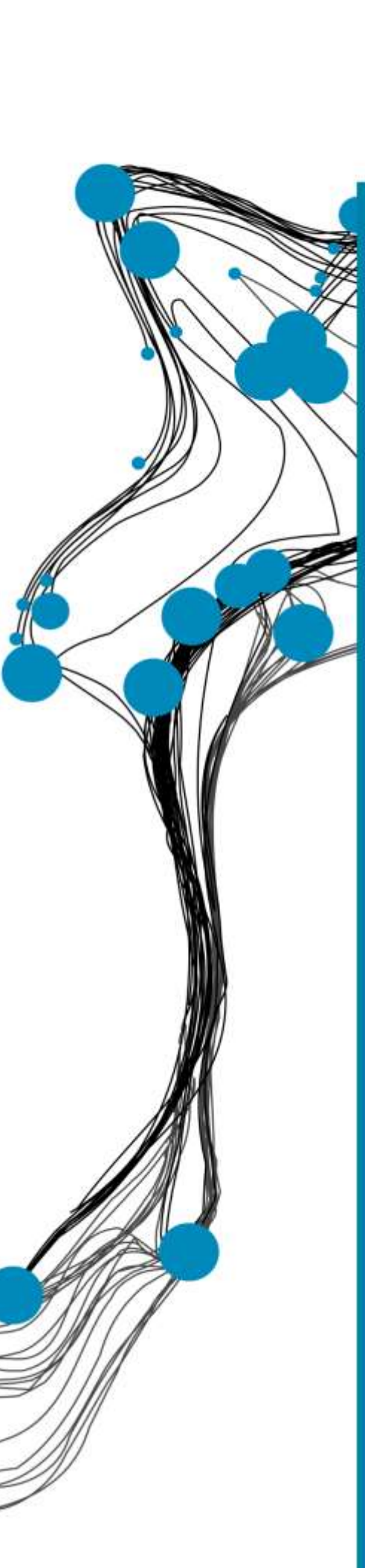

MASTER THESIS BIOMEDICAL ENGINEERING

In vitro modeling of cardiac arrhythmia

Geometrically constrained tissue culture and acoustic pacing with ultrasound

Jeroen Bugter

Science and Technology

Applied Stem Cell Technologies

EXAMINATION COMMITTEE

Dr. V. Schwach

Prof. Dr. R. Passier

Prof. Dr. M. Versluis

31 March, 2020

UNIVERSITY OF TWENTE.

Summary

As cardiac arrhythmias are a large and ever increasing burden on health and healthcare costs, there is a need for more reliable methods of treatment or curing. Development of such treatments is hindered by the lack of reliable *in vitro* models for disease and drug research. This thesis consists of 2 reports of separate studies within the overarching context of *in vitro* modeling of cardiac arrhythmia. Specifically, a method was developed to study re-entry induced by a source-sink mismatch. Using geometrically constrained tissue culture, hESC-derived cardiac microtissues containing a source-sink mismatch were created, and the ideal culture conditions were optimized. Initial readout tests were performed by means of voltage optical mapping and calcium imaging. The second study involves the development of a method for acoustic pacing of *in vitro* cardiomyocytes through ultrasonic pulses. Such a method could provide an alternative to the existing electrical and optogenetic pacing methods, which suffer from cytotoxicity and a lack of excitation depth respectively. Tissues made from hESC-derived cardiac cells were subjected to ultrasonic pulses of various frequency and pulse duration. The responses to the acoustic stimulation were measured through brightfield microscopy recordings. Various observed types of response were catalogued. While actual pacing was at best transiently achieved, the data obtained should provide a start for further development and optimization of this promising method.

Samenvatting

Doordat hartritmestoornissen een grote en immer toenemende last zijn op de algemene gezondheid en zorgkosten, zijn er betere methoden voor behandeling of genezing nodig. De ontwikkeling van dusdanige behandelingen wordt bemoeilijkt door het gebrek aan betrouwbare *in vitro* modellen voor pathologisch en pharmacologisch onderzoek. Deze thesis bestaat uit 2 verslagen over afzonderlijke projecten binnen de overkoepelende context van *in vitro* modeleren van hartritmestoornissen. Om precies te zijn, een methode was ontwikkeld om re-entry geïnduceerd door een source-sink wanverhouding te bestuderen. Doormiddel van geometrisch begrensde weefselkweek zijn hESC-afgeleide hartmicroweefsels met een source-sink wanverhouding geproduceerd, en werden de ideale kweekcondities geoptimaliseerd. Initiële readout methoden werden getest in de vorm van voltage optical mapping en calcium imaging. Het tweede project omvatte de ontwikkeling van een methode voor het akoestisch pacen van *in vitro* cardiomyocyten door ultrasound pulsen. Een dergelijke methode zou een alternatief kunnen bieden voor de bestaande methoden voor elektrisch en optogenetisch pacen, die respectievelijk lijden onder cytotoxiteit en een gebrek aan excitatie diepte. Weefsels gemaakt van hESC afegeleide hartcellen zijn gestimuleerd met ultrasound pulsen van verscheidene frequenties en puls-duraties. De reacties op de akoustische stimulatie zijn gemeten door brightfield microscopie opnames. Verscheidene typen reacties zijn gecatagoriseerd. Alhoewel daadwerkelijk pacen slechts tijdelijk werd bereikt, de verzamelde data zou een startpunt moeten vormen voor verdere ontwikkeling en optimizatie van deze veelbelovende methode.

Acronyms

AF – Atrial Fibrillation

CM – Cardiomyocyte

ECM – Extracellular Matrix

EDTA – Ethylenediaminetetraacetic acid

ES – Electrical Stimulation

FACS – Fluorescence Assisted Cell Sorting

F_c – Centre Frequency

GFP – Green Fluorescent Protein

GT – Geltrex

hESC – human Embryonic Stem Cell

PDMS – Polydimethylsiloxane

PRF – Pulse Repetition Frequency

PRP – Pulse Repetition Period

ROI – Region Of Interest

SR – Sarcoplasmatic Reticulum

US – Ultrasound

VN – Vitronectin

T_p – Pulse duration

Contents

Introduction

Arrythmia is a blanket term referring to any irregularities with the normal heartbeat. This includes an abnormally fast rhythm (tachycardia), an abnormally slow rhythm (bradycardia) or an irregular heartbeat. [*NIH, 2019*] Arrythmias can lead to heart failure, cardiac arrest or a stroke, and have been shown to be a risk factor for cognitive decline and dementia. [*Alonso & Larriva, 2016*]

There are many diseases and conditions that can lead to arrythmia, but atrial fibrillation (AF) is the most common sustained arrhythmic condition. According to a 2010 global burden of disease (GBD) study, it affects an estimated 33 million people worldwide and with rising precedence and incidence. [*Chugh et al. 2013, Rahman et al. 2014*] In general, occurrence of AF is higher in developed nations, due to the increased prevalence of AF risk factors like obesity, diabetes and hypertension [*Chugh et al. 2014*]. Ultimately the accuracy of these estimations is somewhat questionable, as AF can remain asymptotic and undiagnosed. [*Flaker et al. 2005*] The costs for treatment of AF based on 2001 data in the USA alone was estimated to be US$6.64 billion annually. This does not include the costs of possible AF related complications and drug side effects, or the treatment costs when AF is a secondary diagnosis at hospital admission. [*Bajpai et al., 2007*] In summary, arrythmias, in particular AF, are an ever increasing burden on society.

This burden is exacerbated by the fact that persistent arrythmias cannot be reliably cured, instead, treatment of arrythmias mostly relies on continuous management of the symptoms and risks such as through rhythm control drugs and anticoagulants or (surgical) procedures such as cardioversion, catheter ablation or pacemaker implantation. [*Pellman et al., 2015*]

A lot remains unknown about arrythmias which complicates the search for a permanent, reliable solution. The epidemiology of arrythmias is complex and dependent on many factors, like genetics, anatomy, hormones and pre-existing medical conditions, but also more broad concepts as sex and ethnicity. [*Rane & Patton, 2015*] AF is more common in men and among white ethnicities, while sudden cardiac death disproportionally affects black ethnicities and long QT syndrome mostly affects men before puberty, but women after puberty. Research into these factors and their relation to the various arrythmias is complicated by the lack of proper disease models. Investigation of arrhythmic mechanisms is currently performed using *in silico* models [*Zhou et al., 2018*] or *in vivo* animal models. [*Clauss et al., 2019*] Unfortunately *in silico* models require verification and optimization with *in vivo* models and animal models of cardiac diseases are inherently flawed, due in part to the large variation in cardiac anatomy and electrophysiology between various species, limiting the reproducibility of results and possible applicability of the results to the human heart. [*Clauss et al., 2019*]

Therefore a need exists for suitable *in vitro* models using human tissue to properly explore the mechanisms, the genetics or other external factors and possible treatment of arrhythmias. In this report, two separate experimental studies are outlined contributing toward such a model, namely the use of geometrically constrained tissue culture to investigate re-entry by reflection and the potential of ultrasound pulses to be used for pacing of cardiac tissue.

Modelling re-entry by reflection

The goal of this study is to develop a method for *in vitro* modelling of re-entry through the culture of embryonic stem-cell derived cardiomyocytes in specific shapes.

Specifically, by culturing cardiac cells inside a PDMS shape, a source-sink mismatch is forced. The propagation of action potentials through the tissue could be optically mapped. From these readouts, conduction speed and possibly re-entry can be analysed. Previous experiments already investigated several aspects of this methodology, like the preparation of the shape constructs, what protein coating best promotes cell adhesion and what cell density is optimal for the desired result. To complement this earlier optimization, further tests regarding the coating and co-cultures are necessary. Previously, fibrinogen, Matrigel and vitronectin were tested as possible coatings, with vitronectin being found to be the best choice.

Acoustic Pacing

The goal of this study is to explore the practical possibilities of a system for acoustic pacing: to identify the relevant parameters and their values to accomplish the *in vitro* pacing of cardiomyocytes and to identify the limitations of such a system.

As no previous experiments have been performed and little to no existing literature exists on the application of acoustic pacing *in vitro*, trial-and-error will be the primary strategy to investigate. Stem-cell derived cardiac tissues will be stimulated with ultrasound in an existing setup for ultrasonic experimentation and any responses will be monitored.

Geometrically constrained cardiac tissue culture – Theory

In order to understand the potential use of geometrically constrained tissue culture in *in vitro* modelling of arrhythmias, it is important to understand how an arrhythmia can arise and be sustained.

In a healthy heart, the rhythm and rate are determined by the pacemaker cells. These cells start action potentials. Normal contraction of cardiomyocytes is induced when an action potential reaches the cardiomyocyte from surrounding cells it causes the sodium (Na^+) channels to open, depolarising the cell. This results in an influx of calcium (Ca^{2+}) ions through the voltage dependent L-type channels [*Dobrev & Wehrens, 2017, Priest &McDermott, 2015, Schotten et al., 2011*] This initial increase of Ca^{2+} in the cytosol triggers the release of Ca^{2+} from the sarcoplasmatic reticulum (SR).

During rest, the contractile units of the cardiac cell, the myosin and actin filaments are separated by a troponin complex. The high levels of cytosolic Ca^{2+} initiate contraction by causing by binding troponin C, causing this complex to move away. Myosin can then bind the actin filaments and contract the cell as shown in figure 1.1. Relaxation is achieved by moving cytosolic Ca^{2+} into the SR via sarco/endoplasmic reticulum Ca^{2+}-ATPase (SERCA2a) or through the plasma membrane via the rheogenic Na^+/Ca^{2+}-exchanger (NCX), which transports 1 Ca^{2+} ion outward while moving 3 Na^+ ions inward, an electrogenic process. See figure 1.2 for an overview. The membrane potential is repolarized as potassium (K^+) ions leave the cell through various K^+ channels. Original ion concentrations are restored by the Na^+/K^+ pump.

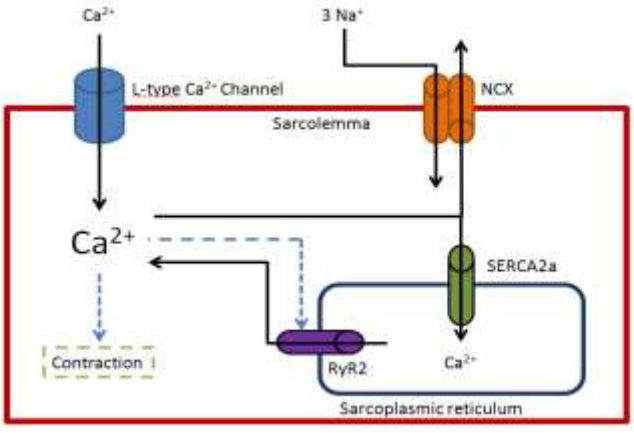

Figure 1.2: Schematic of Ca^{2+} handling in cardiomyocytes after depolarization opened the L-type channels. Black arrows indicate movement of ions, Blue arrows indicate activation.

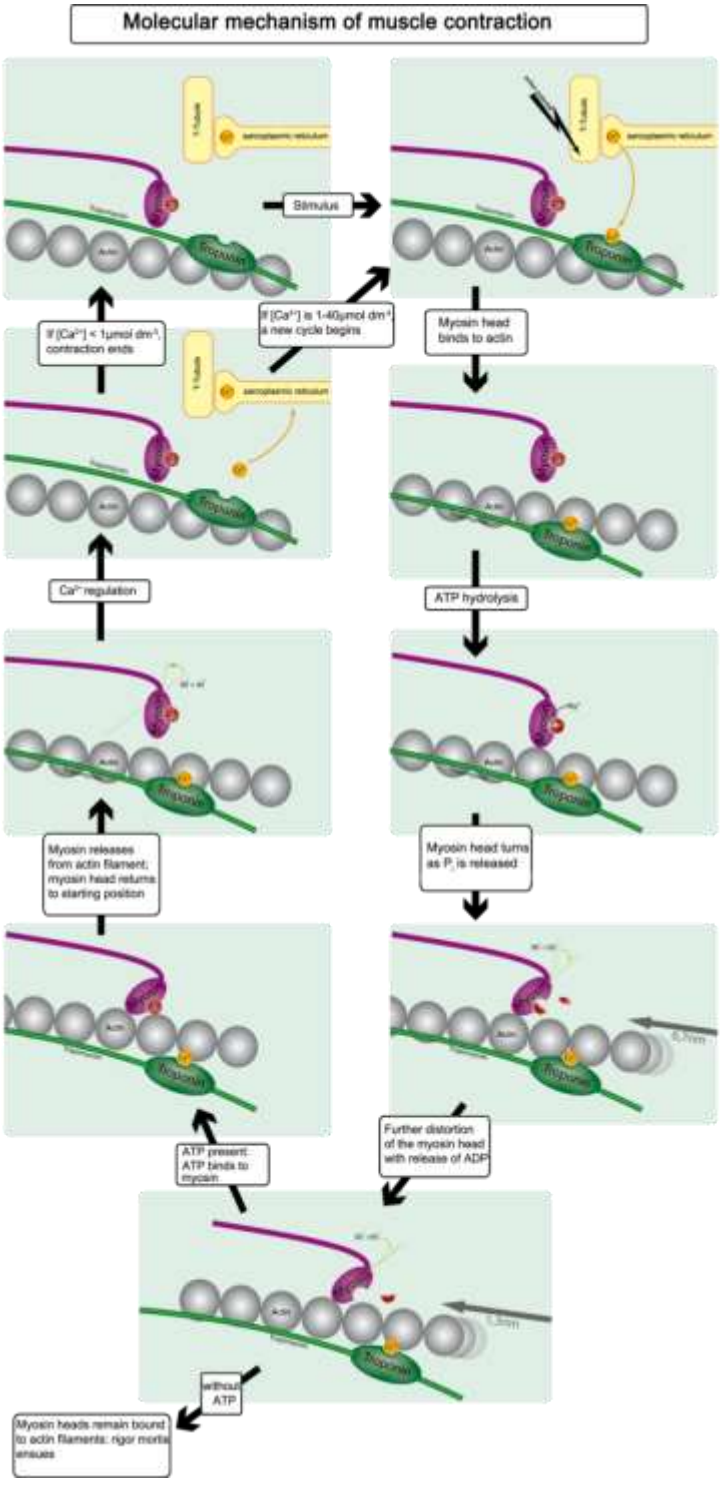

Figure 1.1: Molecular process of cardiac muscle contraction, retrieved from courses.lumenlearning.com, March 4th 2020

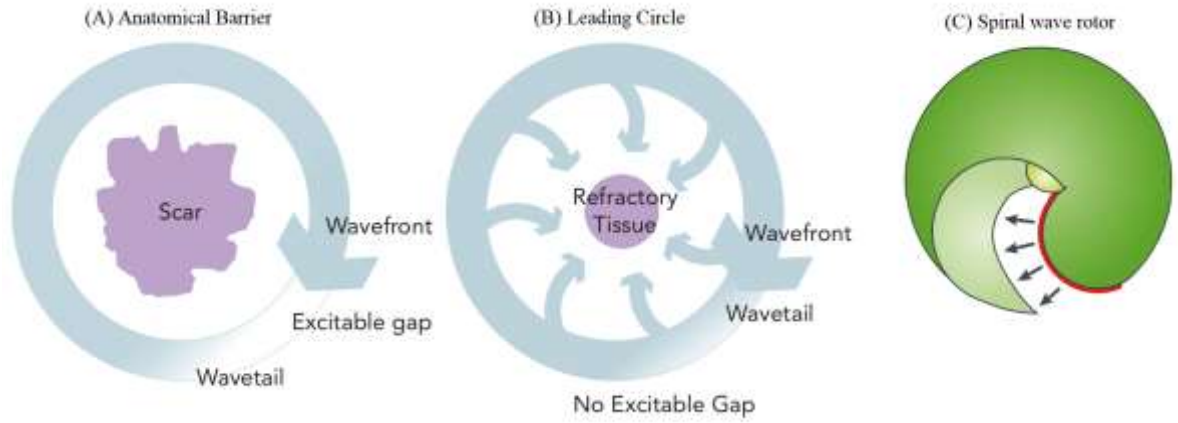

Figure 1.3: The three prominent models of re-entry in atrial fibrillation. A: a non-conductive patch of tissue, such as a scar or necrotic tissue, forces an incoming wavefront to move around it. B: A core of function cardiac tissue is kept permanently in a refractory state by a re-entrant wave, in essence becoming a non-conducting core as in situation A. C: a similar situation as B, but accounting for the variation in conduction velocity based on wavefront curvature, in the centre, this curvature is so great that the conduction velocity is in essence zero, forming a conduction block that's neither anatomical (as in A) or refractional (as in B). [Gonçalves, 2018]

Arrhythmia

Arrhythmias arise due to disturbances in this system. A sustained tachyarrhythmia like AF arises by a combination of a trigger of action potentials outside the regular cardiac pacemaker system and a substrate able to sustain the arrhythmia. Commonly accepted triggers are ectopic foci, where abnormalities in Ca^{2+} handling in the cardiomyocytes causing depolarizations outside the normal cardiac rhythm [*Voigt et al., 2012, Voigt et al., 2013, Beavers et al., 2013, Heijman et al., 2014*], and the phenomenon of re-entry [*Allessie et al., 1977, Nattel, 2002, Pandit & Jalife, 2013, Waks & Josephson, 2014*], the latter being of particular interest in this study.

A portion of tissue undergoing an action potential causes nearby tissue to do the same: the action potential is propagated through the tissue. This propagation will here be referred to as an excitation wave. Re-entry involves the propagation direction of an excitation wave through the cardiac tissue looping back onto itself. In other words, the pacemaker signal re-exciting that part of the tissue it originated from. This creates conduction loops, where a section of tissue is continuously exciting itself, with no input from the cardiac pacemaker. [*Nattel, 2002*] The possibility of re-entrant waves being able to exist is heavily dependent on the substrate, i.e. the tissue itself. If cardiac tissue is still refractory when a new wavefront arrives, the wave would dissipate. Thus, in order to sustain this self-exciting loop, the refractory period needs to be really short relative to the conduction velocity of an excitation wave.[*Allessie et al., 1977, Waks & Josephson, 2014*] Given a substrate able to sustain it, several models of re-entry have been formulated based predominantly on *in vitro* and *in silico* studies, see figure 1.3. In essence, re-entry requires a form of conduction block that forces a change in the propagation direction. In the models of figure 1.3, such blocks are introduced by anatomical abnormalities such as scarring or necrosis, refractional cardiac tissue, or extreme conduction retardation due to the curvature of the wavefront.

Structural remodeling

To further complicate matters, arrhythmias have a negative impact on the cardiac tissue, resulting in various remodelling processes that reinforce the pathological mechanisms of arrhythmias. [*Nattel &*

Harada, 2014] The electro-physiological systems of cardiomyocytes, the autonomic innervation of the heart and the very structure of the cardiac tissue; all are subject to change during sustained arrhythmia, the latter being the most relevant for this study. Structural remodeling occurs mostly through fibrosis. [*Nattel & Harada, 2014*] Cardiac fibrosis involves the increased deposition of extracellular matrix components (ECM), including collagen I and fibronectin, in combination with a reduced degradation. [*Pellman et al., 2010*] In fibrotic atria, cardiomyocytes are further separated from each other and the fibroblasts and ECM form a conduction barrier. [*Pellman & Sheikh, 2015*] Cardiac fibrosis is caused by a variety of factors, such as old age or old age-related cardiac pathologies like myocardial infarction, cell stretch (which can be caused by arrhythmias) and oxidative stress. [*Pellman & Sheikh, 2015, Youn et al., 2013*] Several known arrhythmia risk factors like age, hypertension, diabetes mellitus, obesity and heart failure each involve development of cardiac fibrosis. [*Yang et al., 2017, Russo & Frangogiannis, 2016, Dzeshka et al., 2015*] Structural remodeling has been observed in dogs, sheep, pigs, rabbits, goats and humans alike, but differences exist in the nature of remodeling. [*Nishida et al., 2009*]

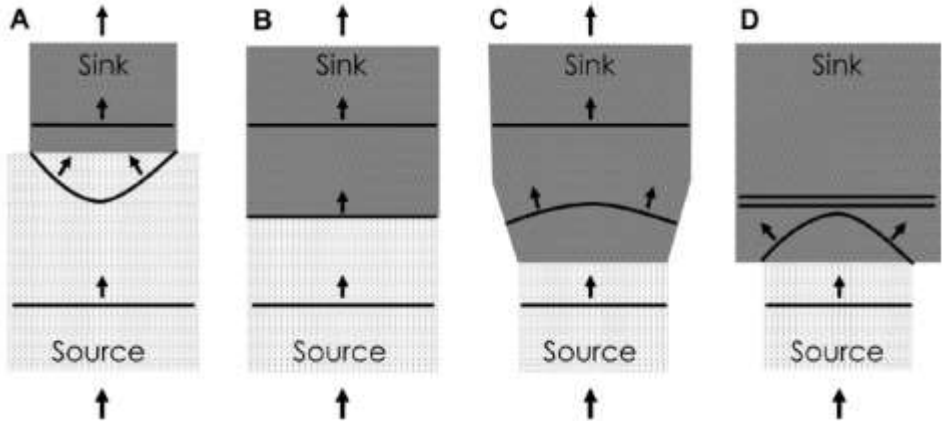

Figure 1.4: "When the source volume is larger (A) or the same (B) compared with the sink volume, activation proceeds because there is sufficient electrical current to activate myocardial cells in the distal direction. When the source volume is smaller than the sink volume, however, the activation wavefront slows (C) or blocks (D) (the latter phenomenon is denoted by the double black line) because there is less electric current available to activate myocardial cells in the distal direction." [Ciaccio et al., 2018]

New theories to be modelled: Re-entry by reflection

Another possible source of re-entry less established as the ones in figure 1.3 is re-entry by reflection due to source-sink mismatch. In regions of heterogeneity in volume of the substrate a source sink mismatch arises, see figure 1.4. [*Ciaccio et al., 2018*] When a wave front traverses from one region with to a region with relatively more volume, conduction will slow, due to the resultant curvature in the wave front, similar to the rotors discussed in figure 1.3C.[*Fast et al., 1997*]

When this difference is extreme enough, the conduction will be so slow a functional conduction block arises. If the refractory period of the region of origin is short enough, the wavefront can reverse direction and re-excite the region of origin – re-entry. The necessary regions of spatial heterogeneity could arise around the edges infarctions, where the necrotic tissue is unable to conduct the wavefront, or in areas with severe fibrosis, as might occur due to structural remodelling. Most research about this model of re-entry has been done by activation mapping in post-infarction canine hearts, and verification in human models is lacking.

In vitro models of arrhythmia

Primary human cardiomyocytes are both difficult to obtain and non-proliferative. These facts have long hindered the development of *in vitro* models. More recently however, various methods have been developed and optimized for the differentiation of cardiomyocytes from human pluripotent stem cells (hPSCs).[*Schwach & Passier, 2016*] Current research efforts are focused on using these cells for use in regenerative medicine or in models of cardiac development, disease or cardiotoxicity. [*Brandão et al., 2017 Park et al., 2018*] These models currently suffer from one main limitation: cardiomyocyte immaturity. These hPSC derived cardiomyocytes have the morphological characteristics and gene expression typical of foetal cardiomyocytes. This limits how representative the models can be for a mature, *in vivo* human heart. Regardless of this limitation, hPSC-CM based models still have a distinctive advantage over the current animal models.

Some effort has already been put into modelling arrhythmias using hPSC-CMs. The rotor re-entry of figure 1.3C was demonstrated *in vitro* using cardiomyocytes derived from embryonic stem cells. [*Laksman et al., 2017*]Genetically modified induced PSCs have been used to study genes related to inherited arrhythmias. [*Bezzerides & Zhang, 2017*] Engineered tissues derived from induced pluripotent stem cells have been used to demonstrate that tissue geometry can induce arrhythmia.[*McNamara et al., 2018*]

Geometrically constrained tissue culture – Methods

Cardiac cell differentiation

Cardiac cells were derived from a transgenic *NKX2.5*$^{eGFP/+}$, *ACTN2*$^{mRuby/+}$ human embryonic stem cell (hESC) line which reliably reports expression of the *NKX2.5* and *ACTN2* genes. Simultaneous expression of these genes is a marker of cardiomyocytes. Expression is reported by green fluorescent protein (GFP) and the red fluorescent mRuby protein. The stem cells were maintained in Essential 8 medium (ThermoFisher) on a surface suitable for tissue culture, coated with 1 µg/cm^2 vitronectin. One day before the start of differentiation, the stem cells were dissociated by incubation with 0.5mM EDTA for 3 min at 37˚C, and reseeded in E8 on a Matrigel coated surface (9 µg/cm^2). At D0, the start of differentiation, the cells were washed with BPEL and the medium was replaced with BPEL containing 20 ng/ml Activin A, 20 ng/ml bone morphological protein(BMP)-4 and 1.5 µM CHIR 99021. On D3, the medium was refreshed with BPEL. The cells were kept in BPEL until D14, refreshing the medium every 3-4 days.

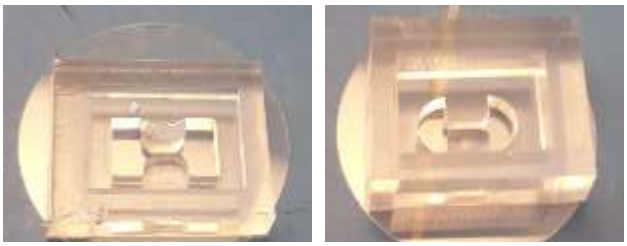

Figure 1.5: Shape constructs from both designs on a 15mm diameter glass coverslip. Left: rectangular double funnel with a shallow reservoir. Right: Rounded double funnel with deep reservoir

Shape preparation

Throughout this project, 2 separate designs for the shapes were used, see figure 1.5. The rectangular double funnel shape can house a tissue of 16.9mm^2, while the rounded double funnel houses a surface of 13.5 mm^2. One shape construct consists of a PDMS shape bonded to a glass coverslip. The PDMS forms the shape on the glass coverslip and also consists of a reservoir to supply medium to the tissue. The shapes were prepared by injection molding using a micromilled acrylic mold and a 10:1 weight ratio mixture of PDMS pre-polymer and curing agent (Sylgard 184, Dow Corning).

Before seeding the cells into the shapes, the glass surface area of the shapes needs to be coated in order to allow cell adhesion. Here vitronectin was compared with Geltrex. Vitronectin was diluted in DPBS in a 1:100 ratio and the shape and reservoir was filled with the solution. After at least an hour of incubation at 37˚C the coating solution was removed and replaced with serum containing medium, so the serum proteins can adhere to the surface to further promote cell adhesion. For Geltrex, a 1:100 solution in DMEM is used.

Seeding cells

After differentiation, the composition of the produced cells was determined with flow cytometry using the GFP fluorescence from *NKX2.5* expression to determine the amount of cardiomyocytes, or the cardiomyocytes were sorted out entirely using Fluorescence Assisted Cell Sorting (FACS). Desired co-culture ratios were prepared by mixing fibroblasts derived from fibroblast-like blastema in with the non-cardiomyocyte population, or, in the case of sorted CMs, just adding enough fibroblasts to the CMs. The

rectangular shapes were seeded with 1.5M cells/cm^2 and 4M cells/cm^2. This amounts to 250k and 664k cells per shape respectively. The rounded double funnels were just used at 4M cells/cm^2, resulting in 540k cells per shape. The cells in shapes were cultured in CM-TDI medium: cardiomyocyte medium supplied with Triiodothyronine, Dexamethasone and Insulin-like growth factor 1 (250-300 µl for the rectangular shapes, 400 µl for the rounded shapes).

After 8, 11 and 14 days of culture, the tissues were subjected to burst pacing. Electrodes were clamped to the reservoir walls, making contact with the medium in the shapes, at opposing sides on the long axis. The tissues were paced using 10ms bursts of 10-15V at 2 Hz.

Calcium imaging

In order to perform calcium imaging, the shapes were supplied with 1:100 solution of 5 mM Fluo-4 AM (Thermo Fisher) in medium. The shapes were incubated for 60 minutes before the dye was removed, the cells were washed and new CM-TDI medium was added. The shapes were then paced as described during fluorescence microscopy. Fluo-4 bound to Ca^{2+} has an Ex/Em of 494/506 nm, which can be recorded using a GFP filter. Using ImageJ, the greyscale intensity was measured at various points in the tissues in order to record the calcium transient.

Optical voltage mapping

Optical voltage mapping was performed externally by N. Harlaar, BSc. at the Leiden University Medical Center (LUMC). Voltage changes at the cell membrane were visualized using an ANEP dye and recorded through fluorescence microscopy.

Geometrically constrained tissue culture – Results

Protein coating

First, the choice of protein coating was optimized by producing shapes coated with either vitronectin (VN) or geltrex (GT). The shapes were seeded with cell mixtures of various ratios of cardiomyocytes to non-cardiomyocytes. To verify the findings regarding optimal cell density previously established, this was first performed using shapes seeded with 1.5 M cells/cm^2. The shapes were seeded with CM to non-CM ratios of 4:1, 3:2 and 2:3. The results are summarized in table 1.1. A successful shape was defined as a tissue where the source/sink mismatch was still present at the time of evaluation.

Table 1.1: Success rates of shapes coated with VN or GT seeded with 1.5 M cells/cm^2 at various CM ratios

Ratio CM:nonCM	Coating	D9	D12
4:1	VN	2/2	0/2
	GT	1/2	0/2
3:2	VN	1/2	0/2
	GT	2/2	0/2
2:3	VN	0/2	0/2
	GT	0/2	0/2

All tissues compacted over time, compacting towards the isthmus and detaching from the outer edges, though the extent of compaction varied considerably. Tissues where the compaction was so extreme as to eliminate the source-sink mismatch or to break the tissue, were deemed failures. See figure 1.6 for examples. The VN 2:3 shape in this figure is an example of a failed tissue. Furthermore tissues that did not respond to burst pacing were also considered failures.

None of the 1.5M cells/cm^2 shapes were maintainable for 12 days. The choice of protein coating did not seem to affect the long term prospects of the tissues, though some differences were visible. GT coated

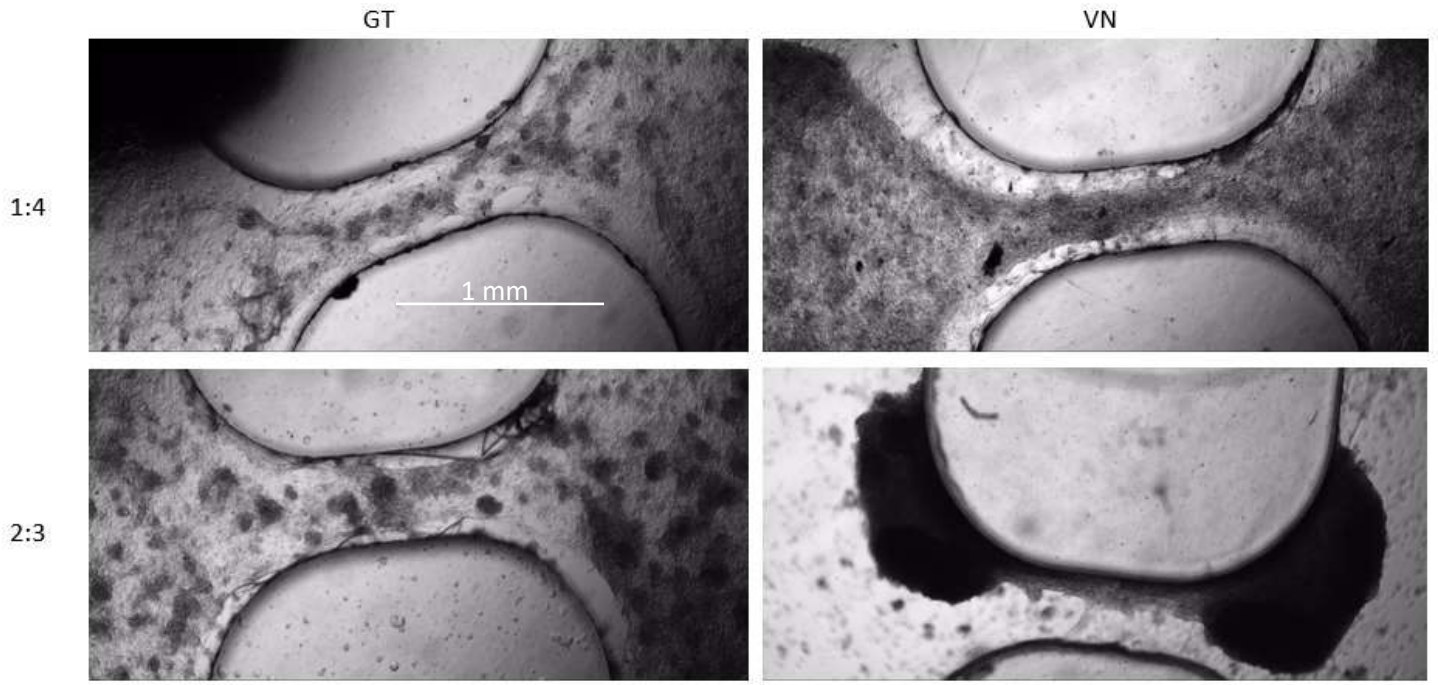

Figure 1.6: Rectangular double funnels seeded with 1.5M cells/cm^2 9 days after seeding, with various protein coatings and CM to non-CM ratios. The shape on the lower right, with VN coating and 2:3 cell ratio is an example of a failed tissue due to collapse.

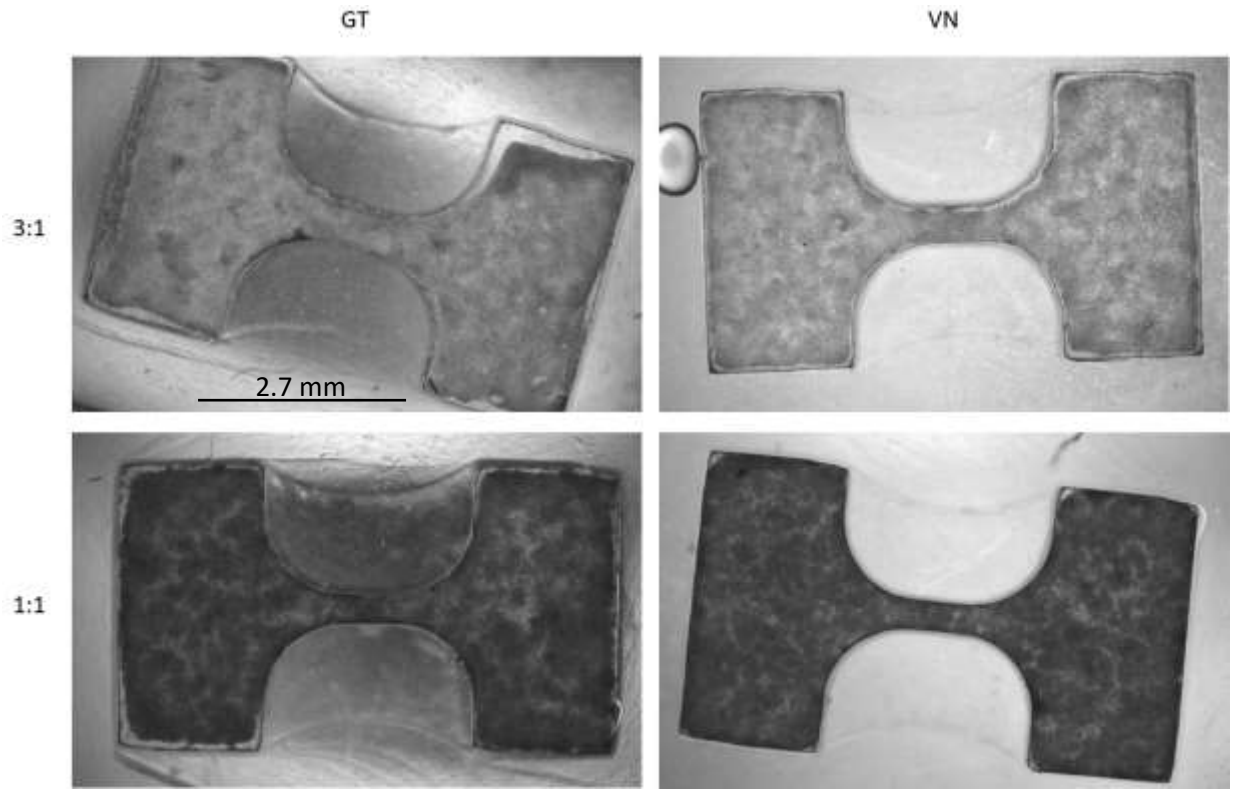

Figure 1.7: Shapes coated with VN or GT, seeded with 4M cells/cm² at 3:1 and 1:1 CM to non-CM ratios. D1 after seeding

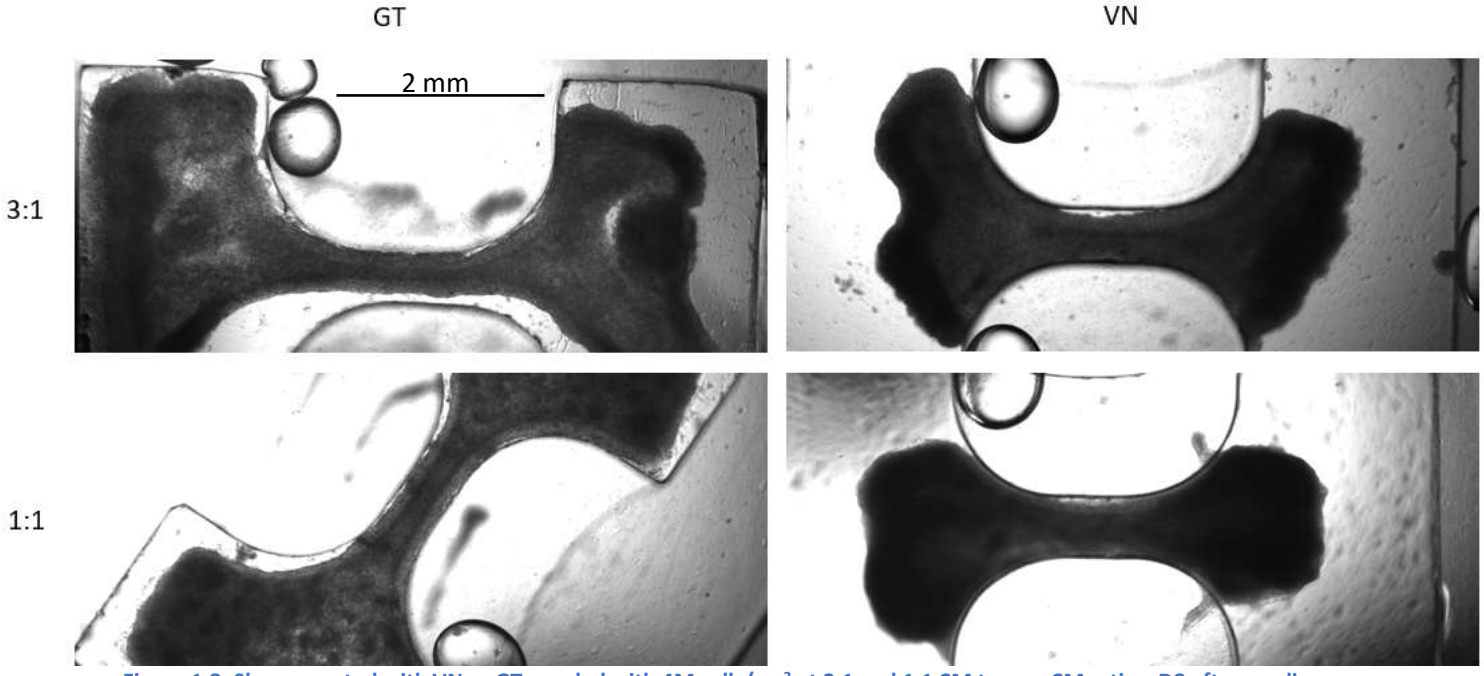

Figure 1.8: Shapes coated with VN or GT, seeded with 4M cells/cm² at 3:1 and 1:1 CM to non-CM ratios. D8 after seeding

shapes were less uniform compared to VN shapes. Conversely GT covered shapes suffered less from compaction and detachment and failed mostly due to unresponsiveness to burst pacing. Best results were obtained with the 4:1 and 3:2 CM to non-CM ratios. To account for the possibility that the low seeding

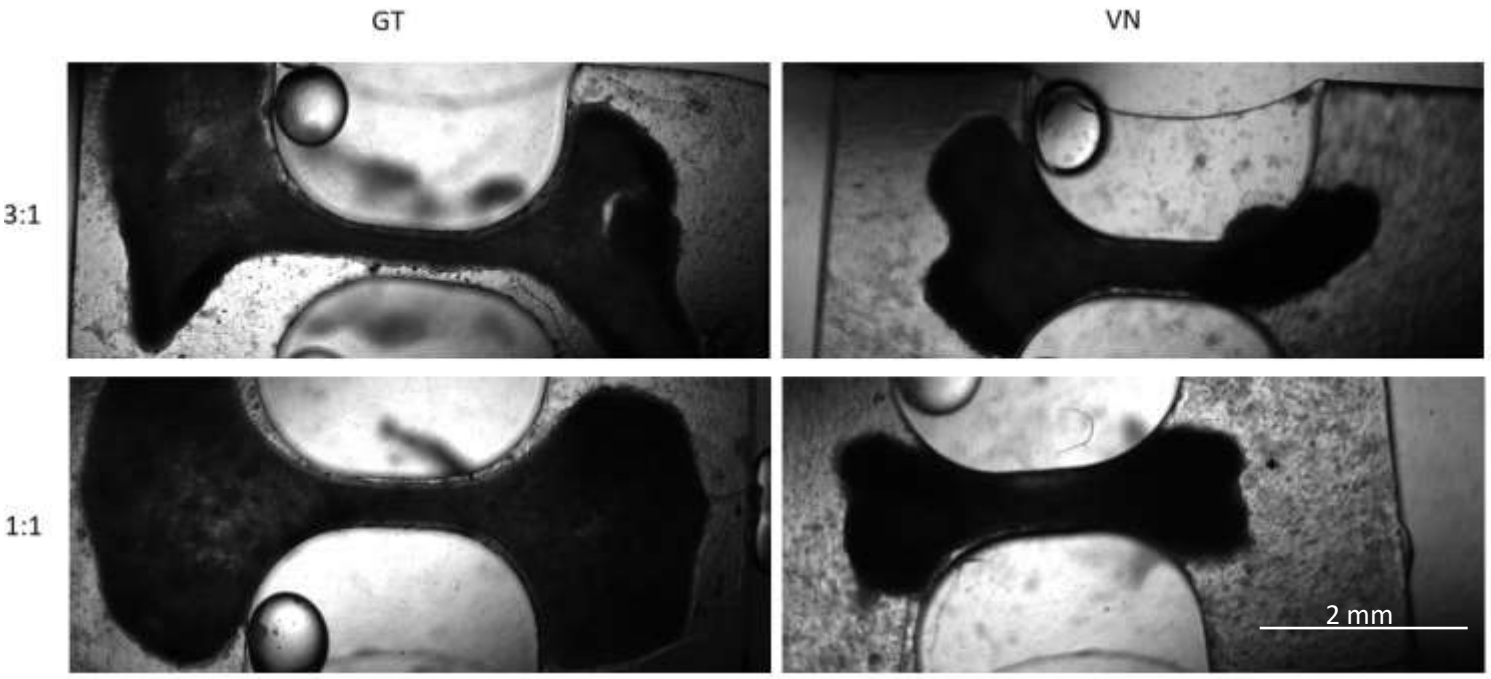

Figure 1.9: Shapes coated with VN or GT, seeded with 4M cells/cm² at 3:1 and 1:1 CM to non-CM ratios. D14 after seeding

density caused the tissue failure, the experiment was repeated with 4M cells/cm^2. See figure 1.7, 1.8 and 1.9.

Table 1.2: Success rates of shapes coated with VN or GT seeded with 4M cells/cm² at various CM to non-CM ratios

Ratio	Coating	D8	D11	D14
3:1	VN	2/2	1/2	0/2
	GT	2/3	2/3	1/3
2:1	VN	1/1	1/1	
	GT	2/2	0/2*	
1:1	VN	4/4	2/4*	0/4
	GT	4/5	3/5*	2/5

Again, VN coated shapes attained a better uniformity of the tissue compared to GT covered ones, although the uniformity of the GT covered shapes did improve compared to the 1.5M cells/cm^2 seeded shapes. Compaction of the tissue affected all shapes, already being visible one day after seeding. Nevertheless, tissues in the GT coated shapes retained their shape for longer compared to VN coated shapes. Only tissues of GT coated shapes could be paced after 2 weeks of culture, see table 1.2. While the tissues remained intact for longer, a design-flaw of the shapes hindered long-term survival. Tissues from the same batch did not survive the second weekend of culture, due to rapid evaporation of medium from the reservoirs. The affected data are marked with * in table 1.2.

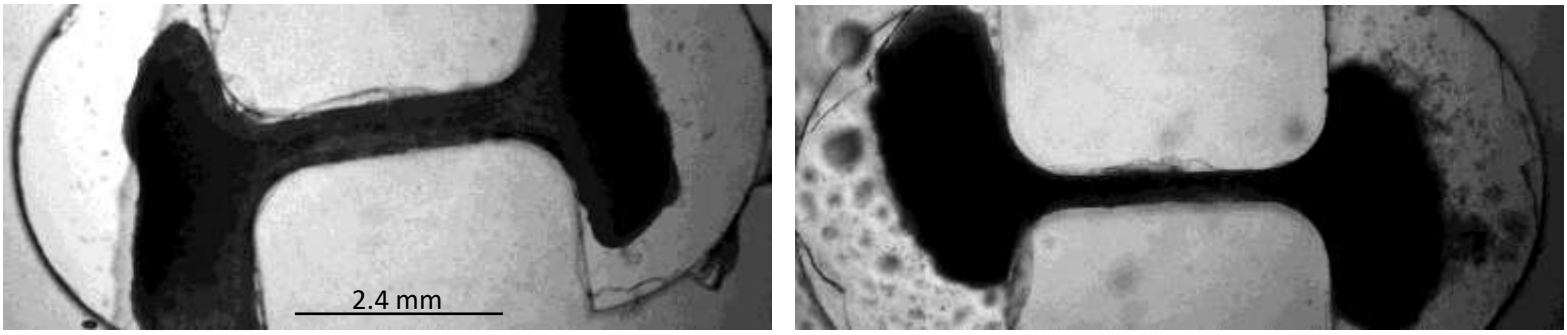

Figure 1.10: Rounded shapes, GT coated seeded with 100% CMs (left) and 70% CMs (right) at 4M cells/cm^2. D8 after seeding.

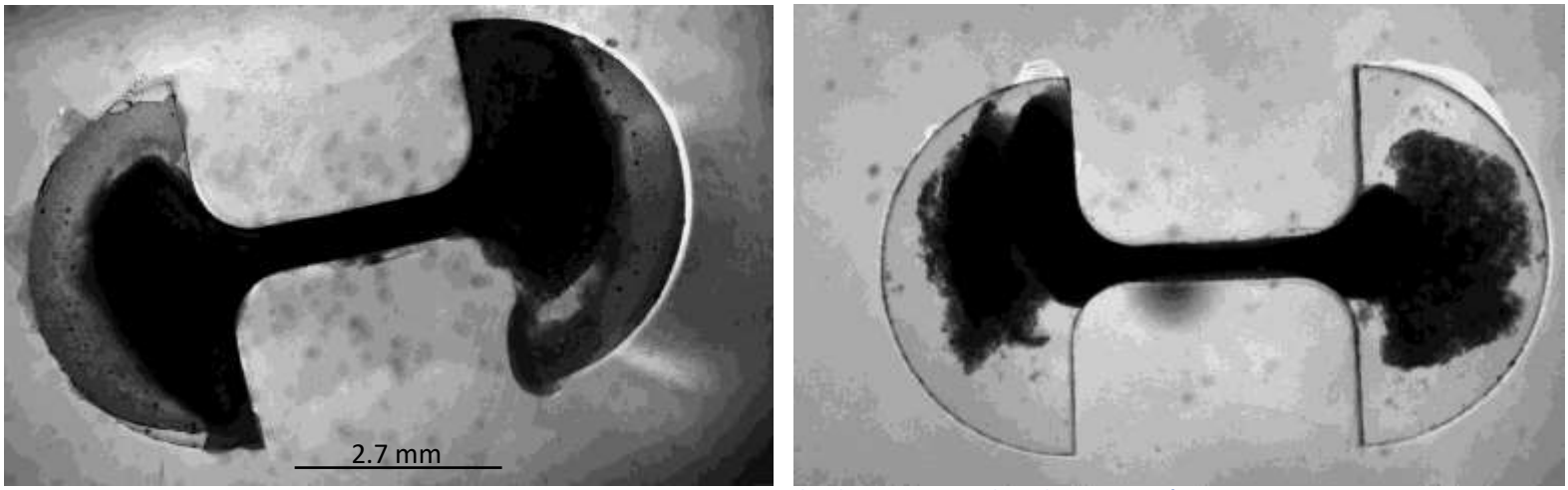

Figure 1.11: Rounded shapes, GT coated seeded with 100% CMs (left) and 70% CMs (right) at 4M cells/cm^2. D11 after seeding.

This prompted the redesign of the shapes, featuring a deeper reservoir. Additionally an adaption to the shape itself was made, featuring rounded sinks instead of rectangular ones. As it was observed that the tissues detach from the corners of the rectangular sinks soon after seeding, the rounded sinks were intended to lessen this effect.

The tissues in all previous experiments consisted of cardiomyocytes and non-cardiomyocytes. Using flow cytometry analysis the CM to non-CM ratio of the differentiation products could be determined, the exact consistency of the non-CM part remains unclear, being some mixture of fibroblasts, epicardial cells, smooth muscle cells etc.. The shapes made with the new design were therefore coated with GT and seeded with 100% pure CMs or a co-culture of 70% pure CMs with 30% fibroblasts. See figure 1.10 and 1.11.

Both culture conditions were well maintainable for 2 weeks. With these results it was decided to move forward using the rounded double funnel, deep reservoir design and GT coating. Furthermore the sorted pure cardiomyocyte and cardiomyocyte-fibroblast co-cultures outperformed the unsorted tissues.

Calcium imaging

Calcium imaging is a valuable tool in analysing *in vitro* models of cardiac tissues. Therefore a calcium imaging protocol was tested using GT coated shapes seeded with an unknown cell mixture of differentiation products, see figure 1.12. The tissues constantly emit fluorescence due to the cells being a *NKX2.5* reporter line. This fluorescence is in the same wavelength as fluo-4 resulting in a constant background signal. Regardless, the signal from fluo-4 is still visible as it is brighter than the background.

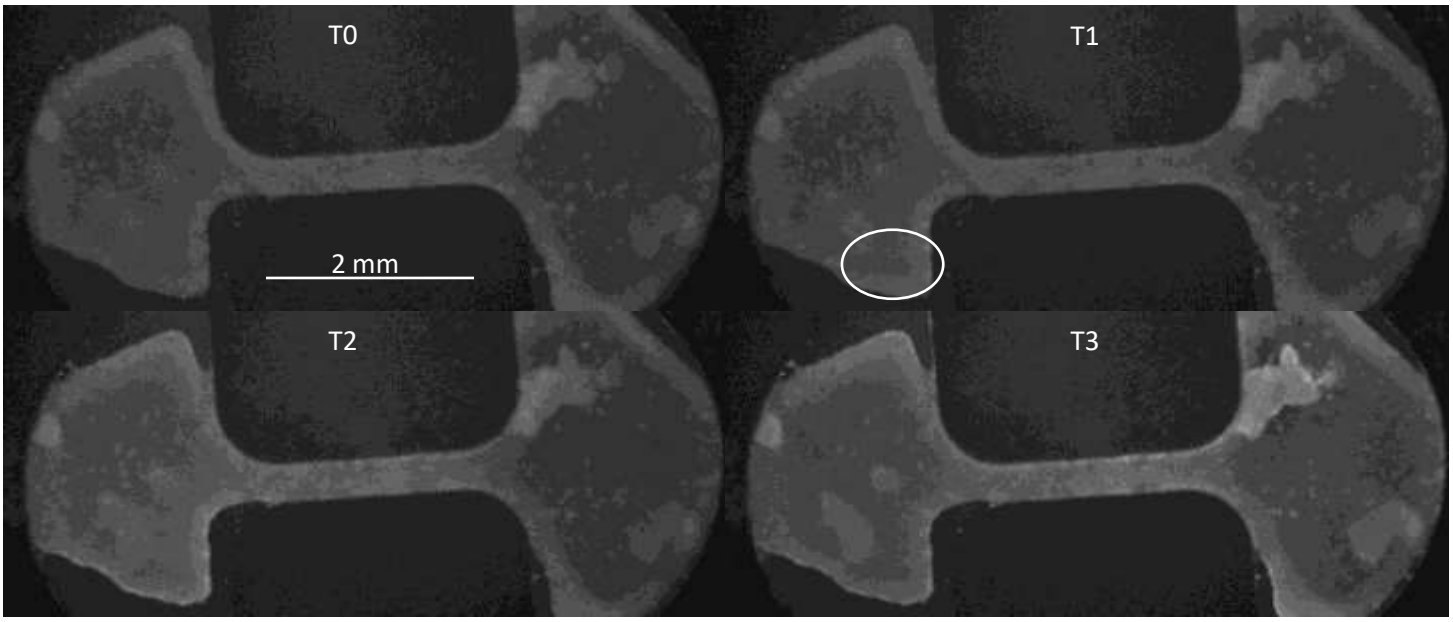

Figure 1.12: Progress of an action potential through the shape (D8) as visualized by Fluo-4. The action potential arises at the left sink, at the ellipsis at T1. It moves through the isthmus at T2 and through the right sink at T3.

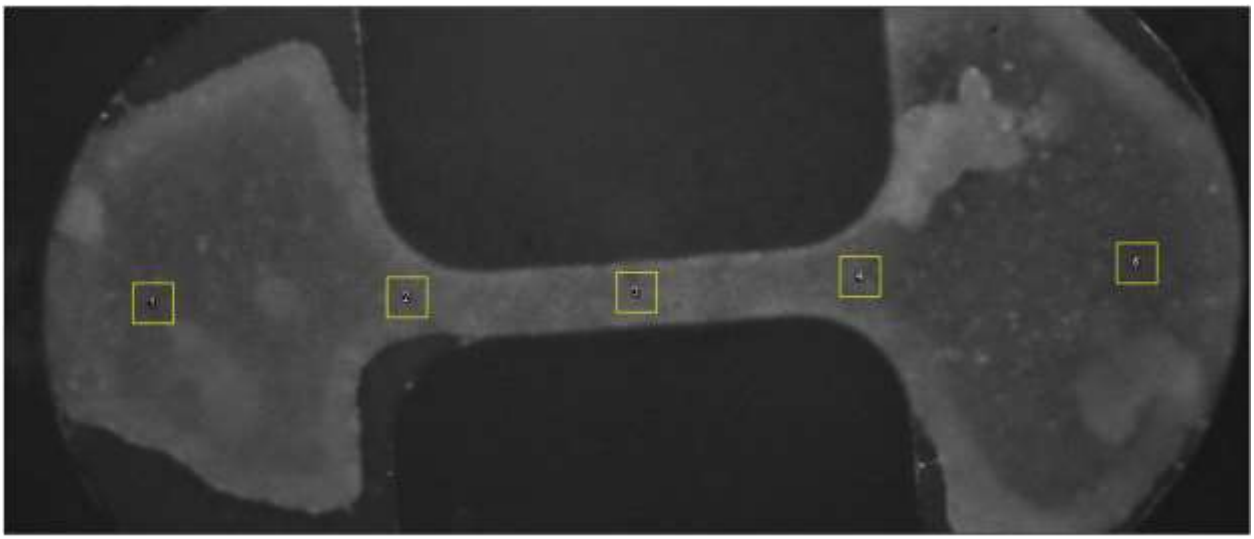

Figure 1.13: ROI placement for calcium transient analysis. ROIs of identical size are placed in both sinks (1 and 5), in the centre of the isthmus (3) and on the isthmus ends (2 and 4).

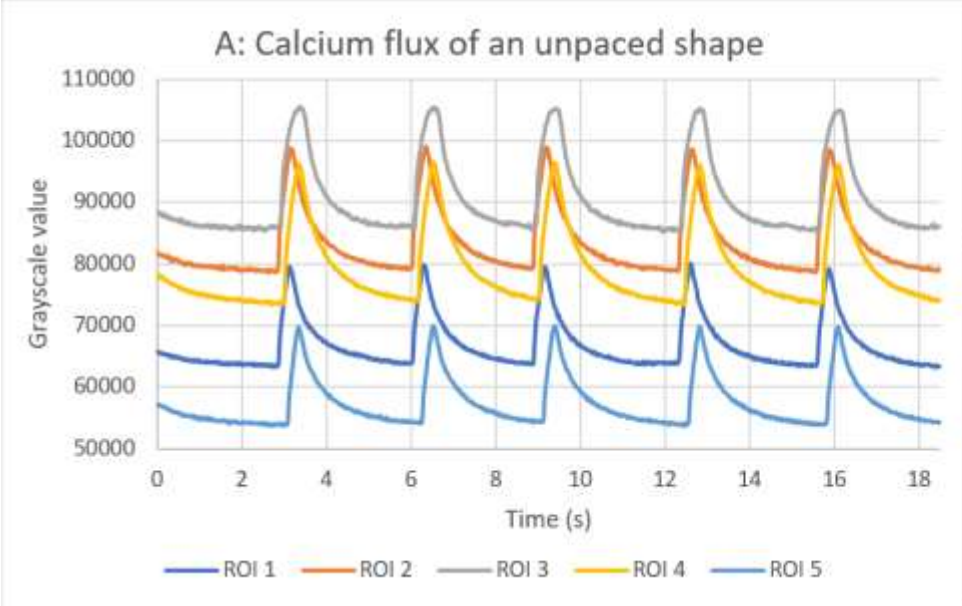

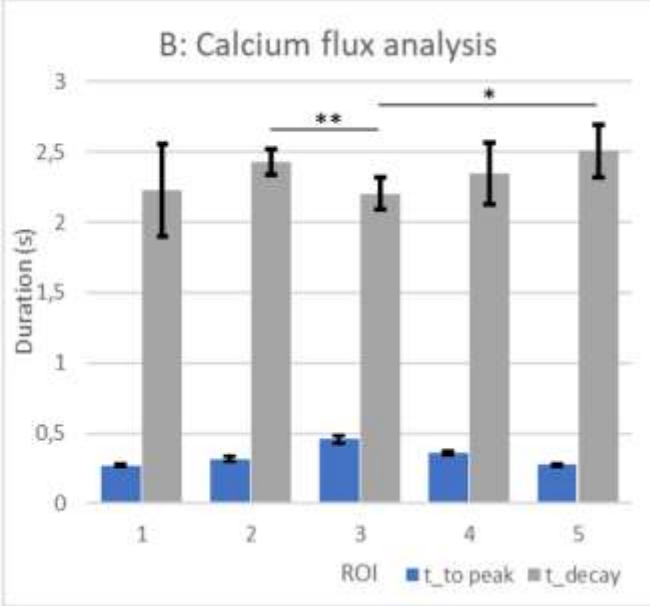

Figure 1.14: Calcium flux (A) and analysis (B) of an unpaced tissue with consistent automaticity. Statistical significance was tested with ANOVA. Statistical significance is not shown for t_to peak as all ROIs are statistically distinct from one another with p < 0,01. For t_decay *: p < 0,05 and **: p < 0,01.

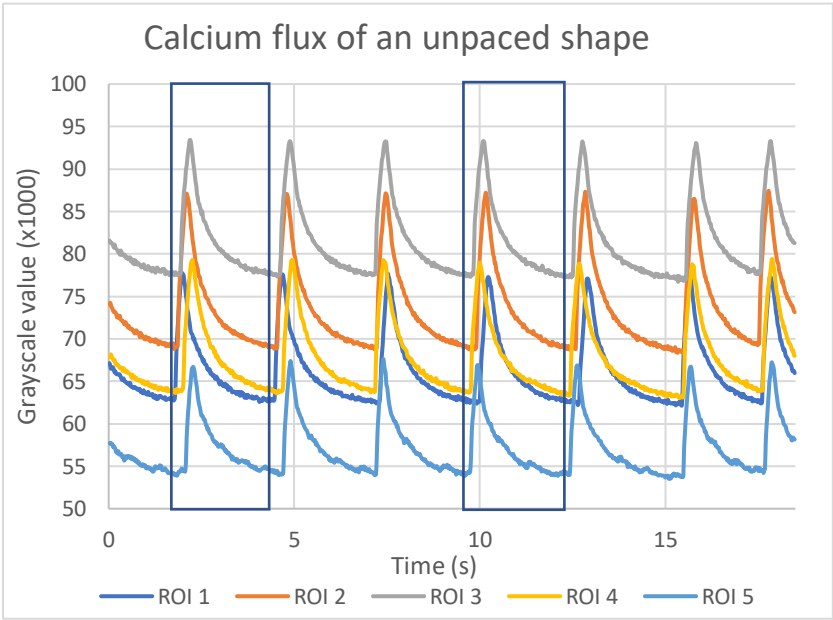

Figure 1.15: Calcium flux over time of an unpaced shape with inconsistent automaticity.

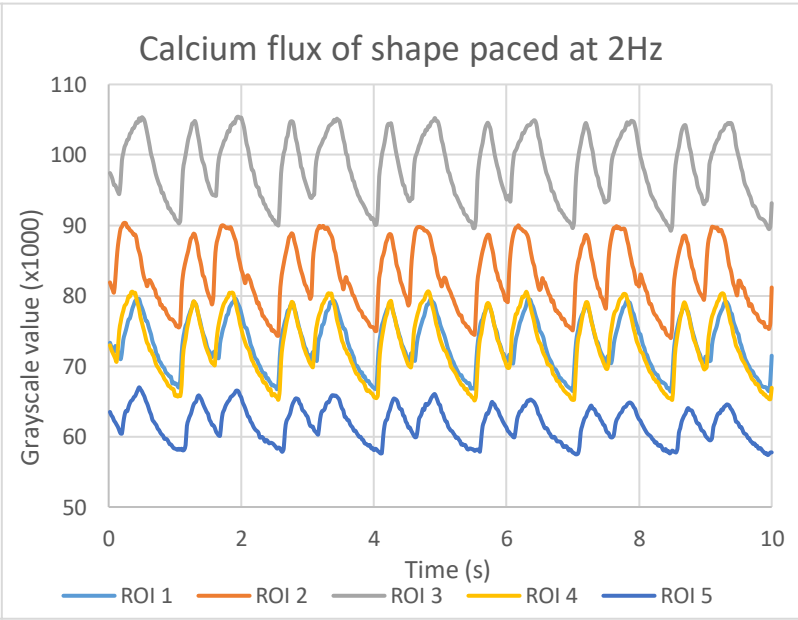

Figure 1.16: Calcium flux over time of a shape paced at 2Hz

Using ImageJ several regions-of-interest (ROIs) were defined in the tissues, see figure 1.13. The calcium flux due to automaticity of two shapes were recorded and analysed as such, resulting in the plots shown in figure 1.14A and 1.15. The tissue of figure 1.14 displayed consistent automaticity, i.e. the origin and direction of the action potential remained the same throughout the recording. This allows for more elaborate analysis of the calcium flux, by obtaining the time between the start of the flux and the peak (t_to peak) and the time it takes for the signal to decay (t_decay), see figure 1.14B. From 1.14A it can be deduced that the stimulus originates around ROI 1 and 2, moving toward 3 (the isthmus) toward 4 and 5.

The t_to peak increased as the stimulus moved into the isthmus, decreasing again when leaving into the other sink. Conversely, the t_decay decreased in the isthmus, increasing again in the sinks.

In contrast to the tissue of figure 1.14, the automaticity of the tissue of figure 1.15 is inconsistent. This is visible when comparing the first contraction with the fourth, indicating that the direction of the action potential has flipped in this case. This hindered further analysis of the calcium flux throughout the tissue. The calcium flux of a tissue paced at 2 Hz is shown in figure 1.16. Here calcium flux appears to occur throughout the tissue simultaneously, making analysis of changes in flux throughout the tissue impossible.

Optical mapping

Rapid automatic contractions of the shapes initially caused difficulties for the optical voltage mapping. This was solved by subjecting the tissues to a 30 min treatment with 10 µM blebbistatin, an inhibitor of muscle contractions. Pacing was not possible due to the very small sizes of the tissues (compared to the large electrode size), instead, the automatic activity of the tissues was mapped. Only 1 tissue with 100% CM could be mapped successfully. See figure 1.17 and 1.18. In this tissue, the signal travels from one end to the other, with an action potential duration of about 220 to 240 ms and with a speed of approx. 10 cm/s, but due to the low amplitude of the signals in the isthmus, this is difficult to visualize. While voltage optical mapping is possible in the shapes, some redesign is necessary to allow for pacing and visualization of the activity in the isthmus

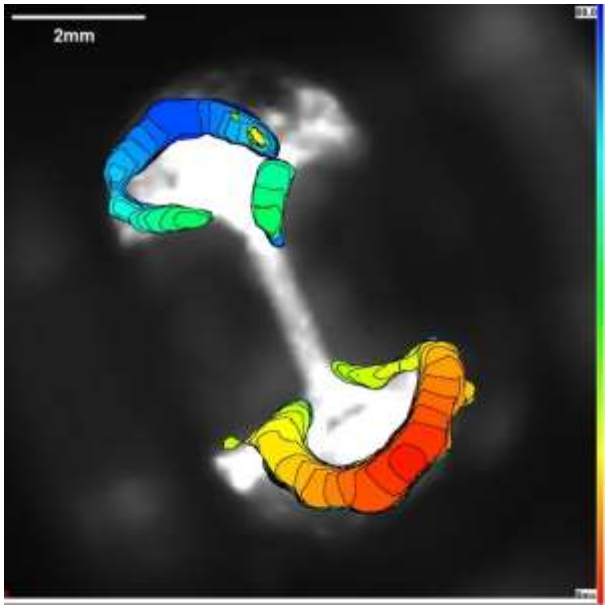

Figure 1.17: Progress of an action potential through a tissue, arising at the lower sink (red) and moving upward (blue). The signal of the isthmus was too weak to be visualized.

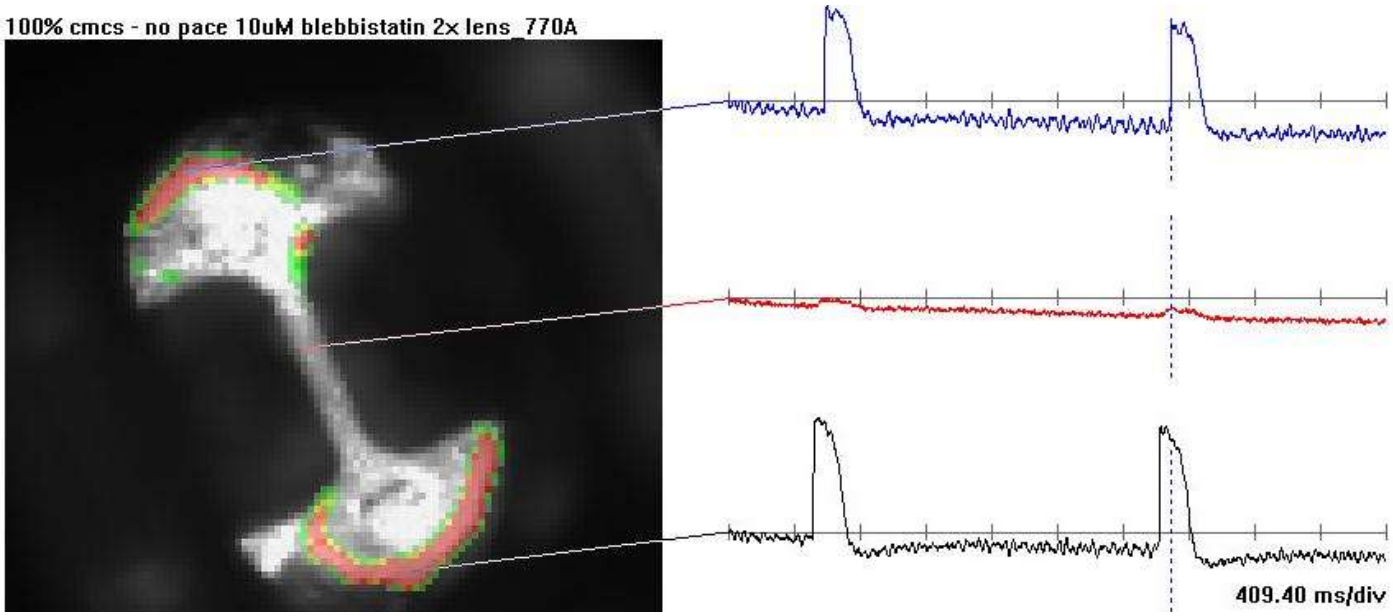

Figure 1.18: Fluorescence signal over time of three separate points (in both sinks and the isthmus) of the tissue during optical voltage mapping

Geometrically constrained tissue culture – Discussion

The data presented here provides a number of insights regarding the optimization of geometrically constrained tissue culture for *in vitro* modelling of cardiac arrhythmias. Firstly, when comparing VN and GT as protein coatings to sustain cardiac cell culture, geltrex was shown to be the better for a culture of 2 weeks. As the electrophysiological connections between the cells are formed at around 8 days of culture, it is important that the tissues can be maintained for at least this period of time, while still maintaining roughly the right shape with the required source-sink mismatch. Tissues on GT did appear to be more clumpy compared to tissues on VN, this inhomogeneity can have adverse effects on conductivity, though the extent of these effects can only be determined with more extensive data from optical voltage mapping.

Interestingly, when comparing co-cultures of CMs and unspecified non-CMs with co-cultures of CMs and fibroblasts, the tissues with a lower CM to non-CM ratio were more robust than tissues with a high ratio. Yet co-cultures of only CMs and fibroblasts were less robust than tissues of pure cardiomyocytes, which is consistent with other findings within the AST group. The fact that cardiomyocytes do not proliferate *in vitro* is what likely causes the apparent inconsistency in results. In the co-cultures with a high CM to non-CM ratio, this ratio only reflects the reality at seeding, as, over time, the non-CMs (fibroblasts, smooth muscle cells, epicardial cells) will proliferate, reducing the ratio during the 8 to 14 days of culture. In the tissues with a low CM to non-CM ratio this likely means that the CM population is overtaken after a while, generating a tissue that has little resemblance to cardiac tissue, but apparently is still fairly robust.

During the optimization of the protein coating, it became apparent that the original, rectangular shape needed to be redesigned in order to more properly facilitate long term tissue culture. Primarily, the now increased reservoir volume allows for the shapes to be left in culture for a couple of days, without medium depletion or evaporation, thus increasing the ease of use. The semi-circular design of the sinks in the new shape is somewhat maintained in the tissue even after compacting. This might help in making the tissues more consistent, though more tests are necessary to see if this benefit indeed exists.

Regarding consistency, it should be noted that the failure rate of the tissues is rather high. Tissues that broke apart before D8 of culture were omitted from tables 1 and 2. The tissues are fragile, especially for the first couple of days after seeding, meaning that great care must be taken when changing the medium, as one can easily disrupt or break the tissue. Similar care must be taken when casting the shapes themselves, as rough edges or gaps along the shape walls can disrupt the structure of the tissue seeded within.

While calcium imaging using fluo-4 is possible on the tissues, the inherent fluorescence of the cell line used, which expresses GFP as a reporter of *NKX2.5*, results in a background signal. Regardless, the fluorescence due to calcium flux can be can still be reliably analyzed. This readout was precise enough to show the direction of the action potential through the tissue and can be used to investigate the peak time and decay time of the calcium flux in unpaced tissues. In paced tissues, all regions of the shape underwent contraction simultaneously, which hinders any investigation into the effect on calcium flux of an action potential moving through a source sink mismatch. To improve on this, the method of pacing needs to be changed in such a way to allow for more localized stimulation. This could be achieved through a small electrode pinned into the tissue itself or through optogenetic pacing.

The optical voltage mapping was performed outside the research group at the LUMC. While these first experiments revealed little regarding re-entry by reflection, they did reveal how to move forward. The small size of the tissues (13.47 mm^2) compared to the electrodes used, made proper pacing of the tissues impossible and complicated the readout, similar to the issues with paced tissues and calcium imaging. To improve this, either the tissues need to be scaled up, or optogenetic pacing needs to be used, as this method requires no electrodes and stimulates cells through light exposure.

Acoustic pacing of cardiac tissue – Theory

Cardiomyocytes *in vitro* derived from embryonic and induced pluripotent stem cells exhibit automaticity, i.e. they contract spontaneously without outside stimuli. [*Kim et al., 2015*] The reason for this automaticity is that these immature cardiomyocytes have properties related to cardiac pace-maker cells, which are able to spontaneously generate action potentials. A researcher has little control over this automatic rhythm. Therefore external pacing is required for *in vitro* models of cardiac tissue and diseases. Pacing of *in vitro* cardiac tissues is not just necessary to control the contraction rhythm of the models, it is also necessary for stem-cell derived heart cells to mature properly. [*Tandon et al., 2009*] Biological pacing, by means of pacemaker cells, has as of yet not been applied, as reliable protocols for pacemaker cell derivation are still being developed. Instead, the most common method to achieve artificial pacing both *in vitro* and *in vivo* has for decades been electrical stimulation (ES). [*Dwenger et al., 2019*]

During ES, the tissue is subjected to short bursts of electrical current, causing depolarization of the cell membrane and leading to contraction, see "Geometrically constrained cardiac tissue culture – Theory'' and figure 1. Unfortunately, ES can cause harmful Faradaic reactions, where electrons are transferred to and from the electrodes which can cause irreversible changes to the chemical environment of the cell, possibly creating chemical species through oxidation or reduction that are detrimental to the tissue. [*Merrill et al., 2005; Williams & Entcheva, 2015; Biesheuvel & Dykstra, 2018*] Furthermore ES cannot be easily be targeted to a specific region of a larger tissue construct, and certain applications would suffer from this lacking spatiotemporal resolution. [*Dwenger et al., 2019*]

The common alternative to ES is optogenetic stimulation. Here, (a portion of) the cardiomyocytes are genetically engineered to express light-sensitive ion channels on the cell membrane. [*Williams & Entcheva, 2015; Jiang et al., 2017*] These cells can then be subjected to light of the specific wavelength the channels are sensitive to, causing them to open and depolarize the cell, leading to contraction. Optogenetic stimulation allows for precise targeting of where the action potential in the tissue should start, and cannot cause detrimental Faradaic effects to occur. However, the required genetic manipulation might have unintended consequences for other functions in the cell, which could bring a level of uncertainty into experiments, furthermore, only cells at or near the surface of tissues can be excited, as light cannot permeate very far. This makes the use of optogenetics limited when investigating thick tissues.

Ultrasonic pulses have been shown to be able to reliably pace *ex vivo* frog and pig hearts. [*Dalecki et al., 1993; Marquet et al., 2016*] Pacing cardiomyocytes using ultrasound, i.e. acoustic pacing, would be a welcome addition to the 2 existing pacing methods, given that ultrasound could be focused deep inside the tissues, while not necessarily requiring genetic modification nor leading to Faradaic effects. To explain how acoustic pacing works, first some general theory about ultrasound should be explained.

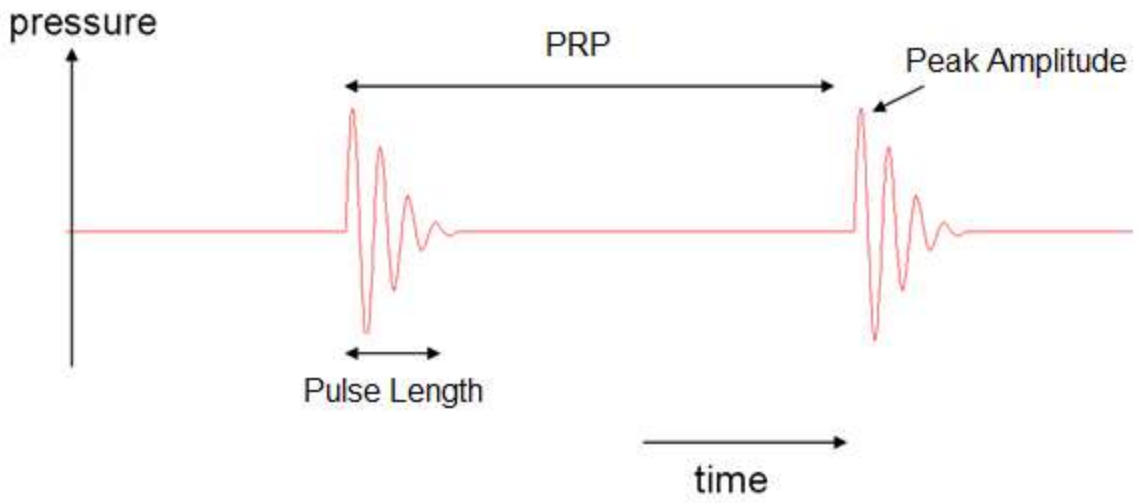

Figure 2.1: Structure of pulsed ultrasound

Ultrasound – General definitions

Figure 2.1 illustrates the pressure within a single point in space subject to pulsed ultrasound. Several parameters have been defined to characterize the ultrasound stimulus. The ultrasound transducer activates for a short time period, the pulse duration (t_p), emitting a soundwave with a certain center frequency (f_c) and peak amplitude. The Pulse Repetition period (PRP) is the time between the onset of 2 subsequent pulses. It is the reciprocal of the pulse repetition frequency. (PRF). [*Hoskins et al, 2010*]

The power delivered by ultrasound to a certain surface is defined as the intensity in W/m^2: [*Prince & Links, 2015*]

$$I = \frac{p^2}{z} = pv \qquad (2.1)$$

Herein, p is defined as the acoustic pressure. Z is the acoustic impedance of the surface, the product of tissue density and the velocity of sound through it. For soft tissues Z= 1.55^{E}6 kg/m^2/s. [*Kubanek et al., 2016*] v Refers to the particle velocity, not to be confused with the velocity of sound. As the intensity of a pulsed ultrasound beam varies over time (as pressure varies over time as well, see figure 2.1) and space (the intensity is not uniform over the entire width of the beam, see figure 2.3), several ways have been defined to describe the average intensity of a pulsed ultrasound beam, see figure 2.2. Spatial peak/average refers to the

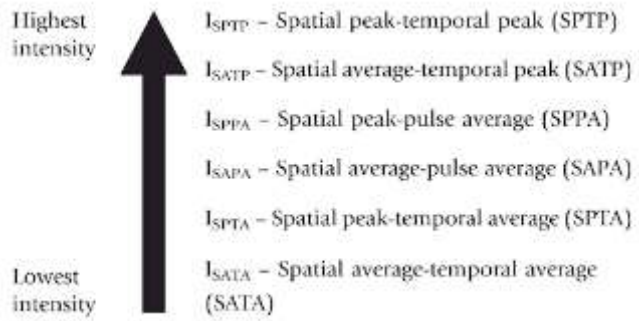

Figure 2.2: Overview of the various ways to describe the intensity of a pulsed ultrasound beam [Gibbs et al. 2009]

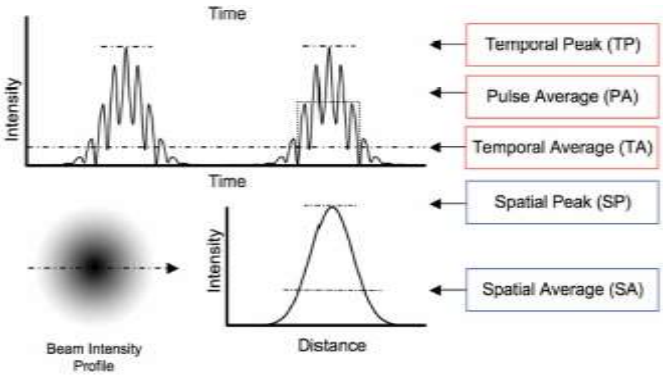

Figure 2.3: Ultrasound variations in time (above) and across the beam (below) [*Nelson et al. 2009*]

intensity variations across beam width. Temporal peak/average refers to the variation across the entire PRP, while pulse average refers to the variation during the pulse duration. I_{SATA} is generally reported. [*Nelson et al. 2009]*

Principles of Acoustic Pacing

While ultrasound pulses have successfully been used to pace *ex vivo* hearts, the exact mechanism through which the pulses are able to accomplish this is currently not fully elucidated.

Ultrasound has been shown to influence certain ion channels, opening them. [*Ibsen et al., 2015; Kubanek et al., 2016*] Particularly interesting is the fact among these mechanosensitive channels is the $Na_v1.5$ channel, see figure 2.4, which is responsible for the influx of Na^+ at the start of an action potential in cardiomyocytes.

The effects of ultrasound on tissue can be divided into mechanical and thermal effects. From several experiments, it has been shown that it are the mechanical effects that chiefly affect whether ultrasound pulses induce contraction, specifically the acoustic radiation force. [*Dalecki et al., 1997]* The acoustic radiation force is the force exerted by an (ultra)sound wave to a point on an object on its path. It is defined as:

$$\left|\vec{F}\right| = \frac{2\alpha I}{c} \qquad (2.2)$$

The acoustic force is F [N], c [m/s] is the sound speed, α [Np/m] is the absorption coefficient of the tissue, and I [W/cm^2] is the temporal average intensity at that spatial location. [*Palmeri et al., 2005*]

Combining these facts leads to the hypothesis that ultrasound pulses exert acoustic radiation force on the cardiomyocytes, which causes the mechanosensitive $Na_v1.5$ channels to open and thereby starting the action potential, leading to contraction.

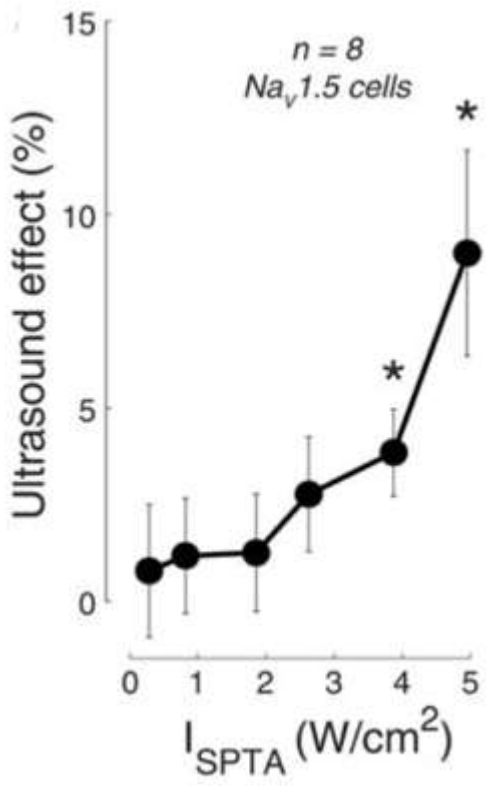

Figure 2.4: The effects of US on $Na_v1.5$ channels as a function of stimulus intensity. The effects were averaged over the voltage steps; mean ± s.e.m. values over cells (n = 8) are shown [*Kubanek et al., 2016*]

Considerations for ultrasound-tissue interactions

In *in vitro* applications, tissue heating and cavitation are important to consider when designing an experiment. As the tissue absorbs ultrasound, it generates heat. If the temperature rises too much, tissue damage can follow. The temperature increase in the medium is dependent on the ultrasound intensity, and the frequency of the pulse, as this determines the level of absorption. This increase can be predicted using the following equation: [*Kubanek et al., 2016*]

$$\Delta T = \frac{\alpha I \Delta t}{C\rho} \qquad (2.3)$$

Where alpha is the absorption coefficient, which is determined by the frequency used, Δt is the time interval of stimulation, C is the specific heat capacity of the medium and ρ is the density of the medium. The absorption coefficient is larger for higher frequencies. The spatial peak, temporal average intensity

(I_{SPTA}) is most closely related to heat generation. FDA regulations require the I_{SPTA} not to exceed 720 mW/cm^2 during *in vivo* ultrasound applications. [*FDA, 2008*]

Cavitation is a non-thermal effect of ultrasound exposure and has 2 subcategories. [*Hoskins et al., 2010*] Non-inertial cavitation refers to the oscillation of gas bubbles exposed to ultrasound. As the pressure of the ultrasound increases, the bubble contracts, during rarefaction, the bubble expands. Non-inertial cavitation requires the presence of certain cavitation nuclei, like solid particles or microbubbles in suspension or bubbles trapped in crevices on solid materials. Non-inertial cavitation is mostly relevant for diagnostic applications of ultrasound, when contrasting agents are introduced which introduce these nuclei.

Inertial cavitation is more destructive. While it only occurs above a certain acoustic pressure threshold, inertial cavitation involves a bubble expanding to its maximum radius and imploding. [*Miller et al., 1996; Izadifar et al*., *2017*] This implosion causes temperature increases, high local pressures and acoustic shockwaves. The main factor that determines whether or not inertial cavitation occurs is the peak negative (or rarefactional) pressure (PNP). The mechanical index (MI), calculated as follows:

$$MI = \frac{PNP}{\sqrt{f_c}} \qquad (2.4)$$

is another parameter used to predict the possibility of inertial cavitation. For MI < 0.7 the physical conditions do not probably allow for inertial cavitation to occur, though exceeding this threshold does not automatically mean biological effects due to inertial cavitation will occur. [*Hoskins et al., 2010*] The FDA has set the upper limit of MI to be 1.9 to minimize tissue damage, for the use of ultrasound in echoscopy or therapeutic applications. [*FDA, 2008*]

In *in vitro* applications, the formation of standing waves should also be considered. [*Secomski et al., 2017*] When ultrasound waves reflect (primarily on water-air interfaces) and the reflected waves run parallel to the incident wave, interference occurs, resulting in a standing wave. This interference hampers the control one has over the acoustic properties of the ultrasound beam.

Acoustic pacing of cardiac tissue – Methods

Cell preparation

Cardiac cells were derived from a human embryonic stem cell (hESC) line. The stem cells were maintained in Essential 8 medium (ThermoFisher) on a surface suitable for tissue culture, coated with 1 µg/cm^2 vitronectin. Either embryonic bodies (EBs) of atrial cardiomyocytes or microtissues of ventricular cardiomyocytes were used.

For the EBs: one day before the start of differentiation, the stem cells were dissociated by incubation with 0.5 mM EDTA for 3 min at 37˚C and seeded at 5 K cells/well in specialized 96-well plates with rounded bottoms, in E8 medium supplied with 0,4 mg/ml PVA and 1:1000 Y27632 ROCK inhibitor. At D0, the start of differentiation, the cells were washed with BPEL and the medium was replaced with BPEL containing 20 ng/ml Activin A, 20 ng/ml bone morphological protein(BMP)-4, 1.5 µM CHIR 99021, 30 ng/ml vascular endothelial growth factor (VEGF) and 40 ng/ml stem cell factor (SCF). On D3, the medium was refreshed with BPEL. On D4 the medium was changed again, with 100 µl BPEL per well containing 1 µM retinoic acid. On day 7, the EBs were collected using biosphere® pipette tips and placed in a rounded bottom 96-well plate (5 to 10 EBs/well) in BPEL and kept in culture for another week before moving on to sample preparation.

For the micro tissues: one day before the start of differentiation, the stem cells were dissociated by incubation with 0.5 mM EDTA for 3 min at 37˚C, and reseeded in E8 on a Matrigel coated surface (9 µg/cm^2). At D0, the start of differentiation, the cells were washed with BPEL and the medium was replaced with BPEL containing 20 ng/ml Activin A, 20 ng/ml BMP-4 and 1.5 µM CHIR 99021. On D3, the medium was refreshed with BPEL. The cells were kept until D14, refreshing the medium on D7, D10 and D13. After differentiation the cells were dissociated with TrypLE 10x and seeded in BPEL in a special 96-well plate with rounded bottoms at 20k cells/well. This plate was then centrifuged at 1100 RPM for 10 minutes. These microtissues were then maintained for 4 to 5 days before moving on to sample preparation.

Sample preparation

The prepared tissues are placed on Mylar membranes using Matrigel. The sample holder is designed to hold round coverslips with a 15 mm diameter. Mylar membranes are glued to polymer rings that fit in this stage using UV-curable glue (Norland optical adhesive). The membranes are placed in a 12-well suspension plate and 10 to 20 ul of Matrigel stock solution (~10 mg/ml) is dispensed on the membranes, and spread around with a pipette tip to coat the membrane. Using a pipette tip widened with a scalpel, about 10 tissues (EBs or microtissues) are collected and dispensed on the Matrigel, with as little as medium as possible. See figure 2.5 for a schematic overview. This way the tissues are close together on the membrane, which improves stability. The Matrigel was then gelated at 37˚C for an hour before adding medium to the wells. The tissues were kept in culture for another 5 to 7 days, to allow the non-cardiomyocytes in the tissues to produce their own ECM to anchor to the gel and membrane better.

Before acoustic stimulation the membranes with tissues were attached to the sample holder using vacuum grease.

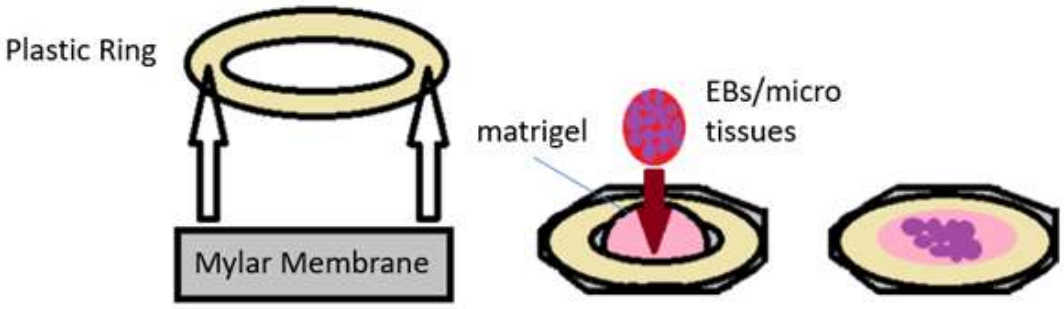

Figure 2.5: Schematic of sample preparation for acoustic pacing

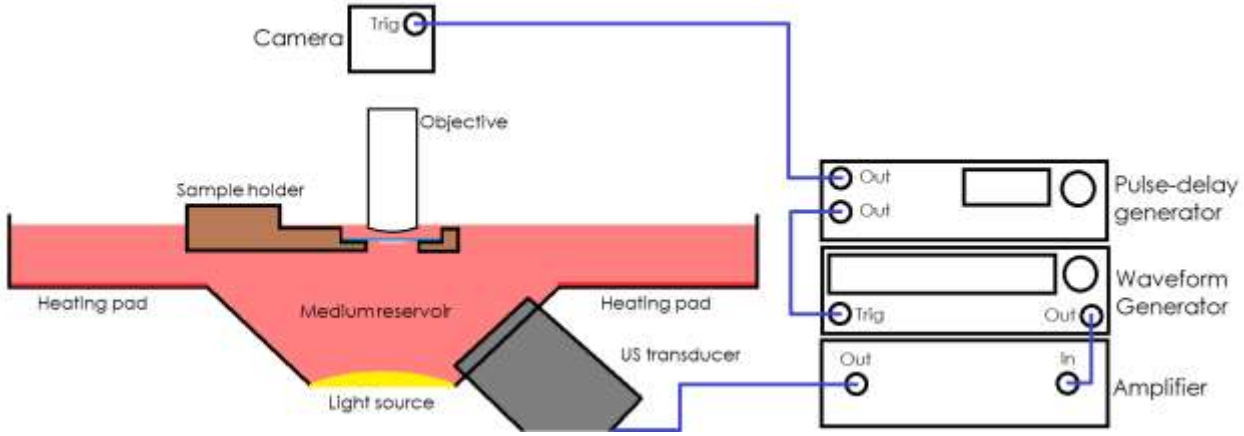

Figure 2.6: Schematic of the acoustic pacing setup

Ultrasound setup

See figure 2.6 for a schematic of the setup for acoustic pacing. The sample is placed on the sample holder in the medium reservoir and submerged in medium. The reservoir contains heating pads and a temperature sensor that allow for the control of medium temperature. The reservoir is located under a microscope and positioned in such a way that the focal point of the 20x objective corresponds with the 1.63 inch (4.14 cm) focus of the 1 MHz (100% bandwidth) ultrasound transducer placed in the wall of the reservoir. Using a hydrophone, this calibration is checked at the start of every measuring day. The ultrasound hits the tissue under an angle, preventing standing waves from forming. A single measurement is essentially a recording of the tissue. This recording consists of an initial waiting time (WT) during which the tissue is not stimulated for 10 or 20 seconds, followed by 40 seconds of ultrasound time (TUS) during which the tissue is subjected to ultrasound pulses and finally another 20 seconds of post ultrasound time (PUS) where no stimulation happens. Thus, one recording contains both the measurement and negative control. The values of WT, TUS and PRF are all programmed into a pulse-delay generator (Berkeley Nucleonics). As the pulse-delay generator is activated, it triggers the camera to record for the total measurement duration (WT+TUS+PUS). After the WT is over, it starts sending triggers at the PRF frequency for the duration of TUS to the waveform generator (Agilent Technologies). In the waveform generator the duration and f_c of the ultrasound pulses is programmed. As triggers from the pulse-delay generator arrive, the waveform generator outputs the pulses to the amplifier (Electronics & Innovation), which finally amplifies the pulses to voltages suitable for the transducer.

Experimental parameters

Tissues were subjected to ultrasound of 0.5, 0.7, 1.0 and 1.5 MHz. The fact that changing the centre frequency also changes the pressure output of the transducer, was not accounted for. See table 2.1 for the corresponding acoustic pressure for each used frequency. This makes asserting the effects of pressure and frequency as separate parameters impossible. Due to limitations of the equipment available, the PRF was kept between 1 and 1.5 Hz and the maximum t_p was 1.2 ms.

Table 2.1: centre frequency and acoustic pressure

f_c (MHz)	p (MPa)
0.5	1.6
0.7	2.8
1.0	3.7
1.5	5.0

Data processing

The raw data obtained during a measurement consists of $\pm 4000\ (Q)$ frames of $1264x1016\ (N \times M)$ pixels, stored in $.tif$ files. Furthermore each measurement comes with a $.xiseq$ file, which contains timestamps of every frame. With use of $MATLAB$ $.avi$ files are made with a framerate of $50fps$. The movies therefore are not based on the timestamps of the $.xiseq$ files. Time domain representation of the results however, are based on the timestamps of the $.xiseq$ files.

Data pre-processing is necessary to correct for two dimensional translational motion. This occurs for example when the camera and sample stage move with respect to each other due to vibrations. Translational motion is detected by using $MATLAB's\ normxcorr2$ function. One needs a template image, in most cases the first frame of a video (f_1), and a frame of interest (f_i). The function slides f_i over f_1. For each position of the frame of interest, the degree of similarity with the template image is quantified. The position with the highest degree of similarity is used to define the dominant translational motion. This results in $\Delta v(direction, t)$ which contains for every timestamp the motion in directions x & y. In some cases the motion is very brief and large. To correct for those movements, motion signal is smoothened by $MATLAB's\ fit$ function with $SmoothingParam = 0.5$. This results in $\Delta v_s(direction, t)$.

After data pre-processing, data processing takes place. It consists of calculating a measure of variance of the frame of interest from the reference frame. From the $.avi$ files, four distinct signals are calculated, see figure 2.7, these are:

1. The uncorrected signal uses frame 1 as reference frame and compares all pixels.
2. The correction with regards to previous frame uses frame $i-1$ to analyze frame i and compares all pixels.
3. The translational motion corrected signal uses frame 1 as reference frame and compares only the pixels that are visible in both frames, by using $\Delta v(direction, t)$.
4. The smooth translational corrected signal uses frame 1 as reference frame and compares only the pixels that are visible in both frames, by using $\Delta v_s(direction, t)$.

The signals vary in terms of used reference frame and motion correction. Generally the first step is selecting the pixels that should be compared, whereafter the frame of interest is compared with the reference frame. The result is an error matrix which contains the differences of all pixels. This error matrix is squared, where after the summation is squared and normalized by dividing with the matrix size.

$$S = \frac{\sqrt{\Sigma \epsilon^2}}{N_{fi} \times M_{fi}} \qquad (2.5)$$

This is a quantification of the change in frames and can be tracked over time for the duration of the recording. In this application, it allows for the detection of contractions of recorded tissues.

Data representation consists of time domain representation, frequency domain representation and region of interest analysis. Short time Fourier transform (STFT) data is extracted by $MATLAB'$s $spectrogram$ function. STFT uses a long time domain signal and analyses multiple shorter time samples from the whole dataset. It is used to detect frequency content changes over time.

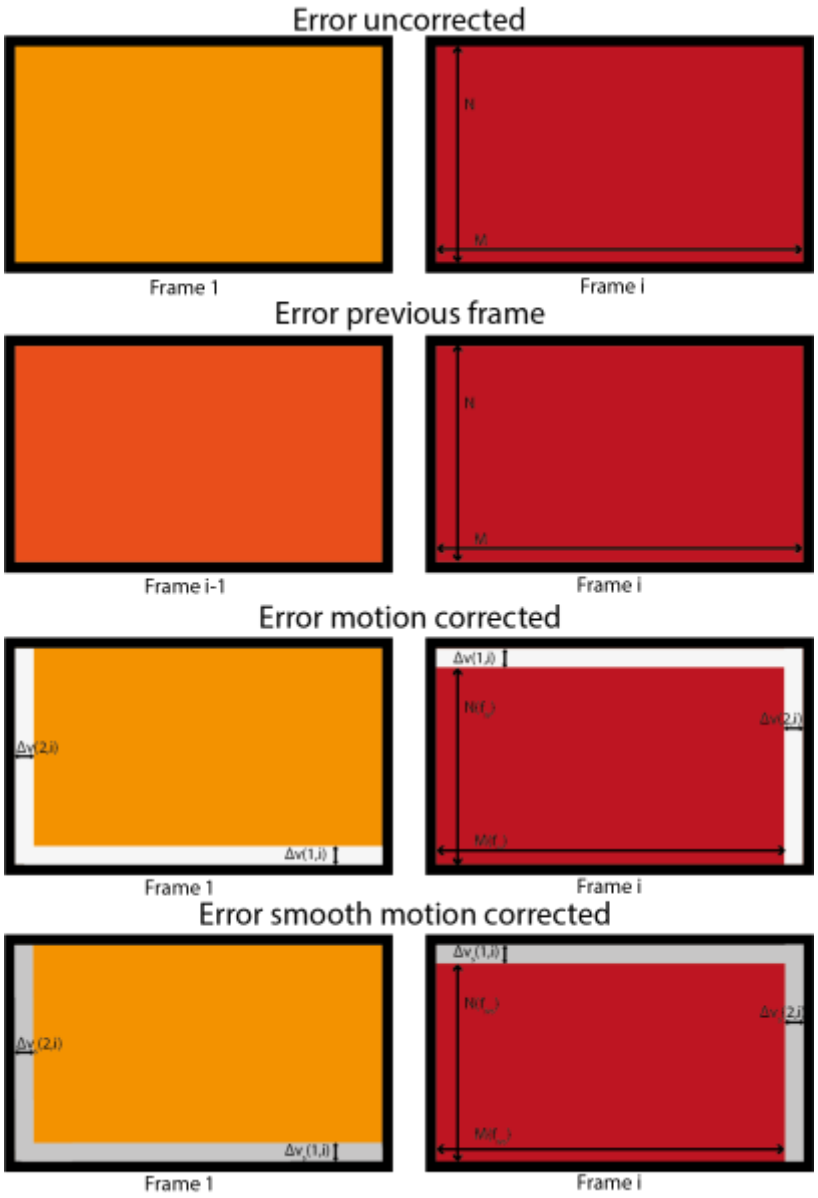

Figure 2.7: Representation of the calculation of change between frames based on the four various pre-processing methods used.

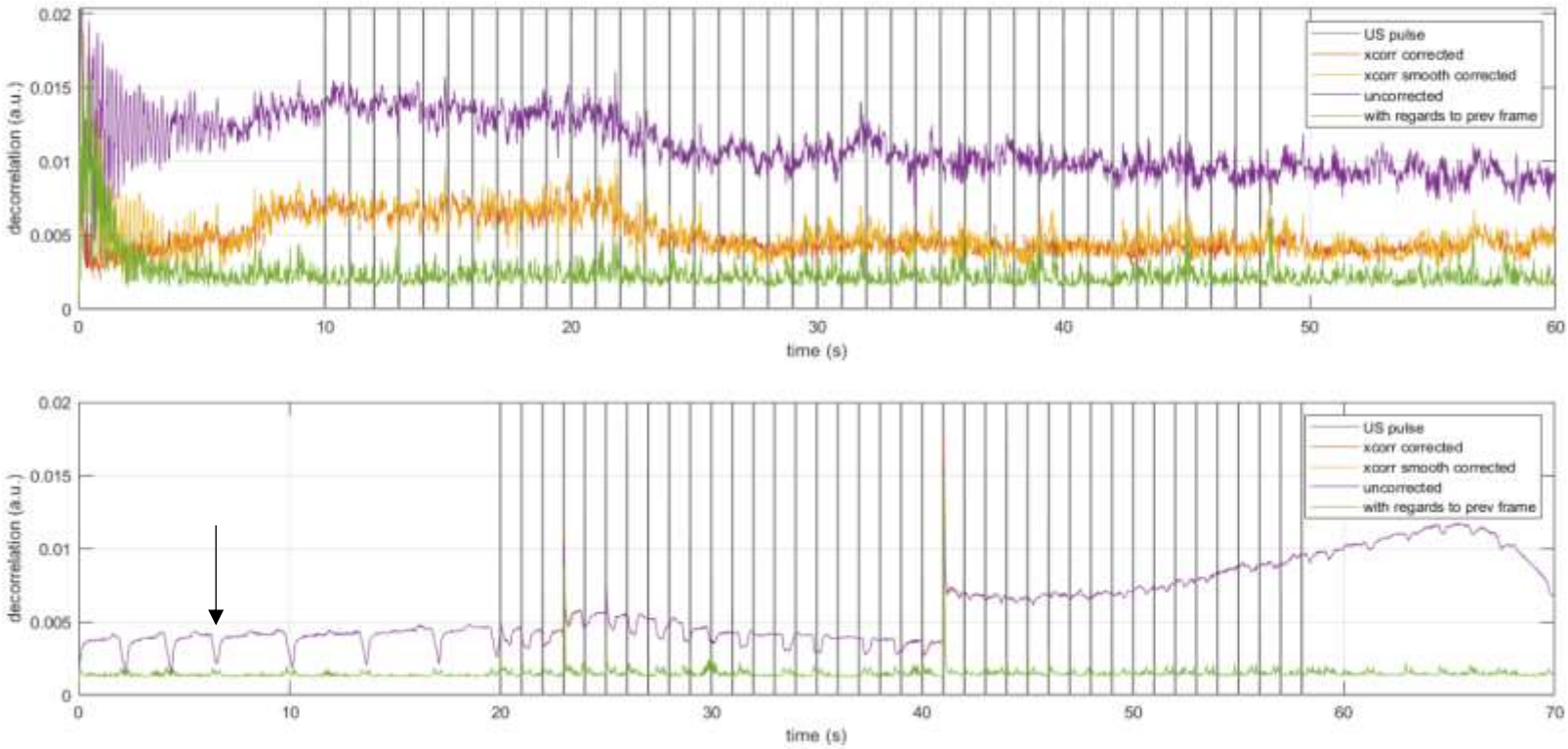

Figure 2.8: Comparison of data processing of a recording of acoustic stimulation of an empty membrane (above) and a membrane with tissue (below), the arrow indicates a contraction. f_C = 1 MHz, t = 1 ms, PRF = 1 Hz

Acoustic pacing of cardiac tissue – Results

In order to verify that the data processing method indeed does register movement from the tissue and not just movement from the mylar membrane, a tissue samples were compared to membranes without Matrigel or tissues, but with lines drawn onto them. See figure 2.8, where the contractions of the tissue are clearly visible from the processed data as opposed to the more random vibrations of the empty membrane.

Various events were observed when stimulating tissues with ultrasound pulses of various f_c and pulse durations. The following events were defined:

- Rhythm increase – Any increase in the contraction rhythm of the tissue during the ultrasound time of the recording, this includes pacing and tachyrhythmia events. See fig. 2.9, 2.10 and 2.11.
- Pacing – The contraction rate corresponds to the PRF of the ultrasound pulses, and the contractions follow the pulses. See fig 2.10 and 2.11.
- Tachyrhythmia – The contraction rate of the tissue increases dramatically following US stimulation, to a rate higher than the PRF of the ultrasound pulses. See fig. 2.10.
- Cavitation – These events appear as bright flashes and brief intense movement on the recordings, resulting in delta-like peaks in the movement plots. While it is not confirmed that these events are indeed cavitations, they do resemble how cavitations appear on video in other studies. See fig. 2.9 and 2.10.
- Disruptions – Events where the tissue is destroyed during ultrasonic stimulation. See fig.2.9.

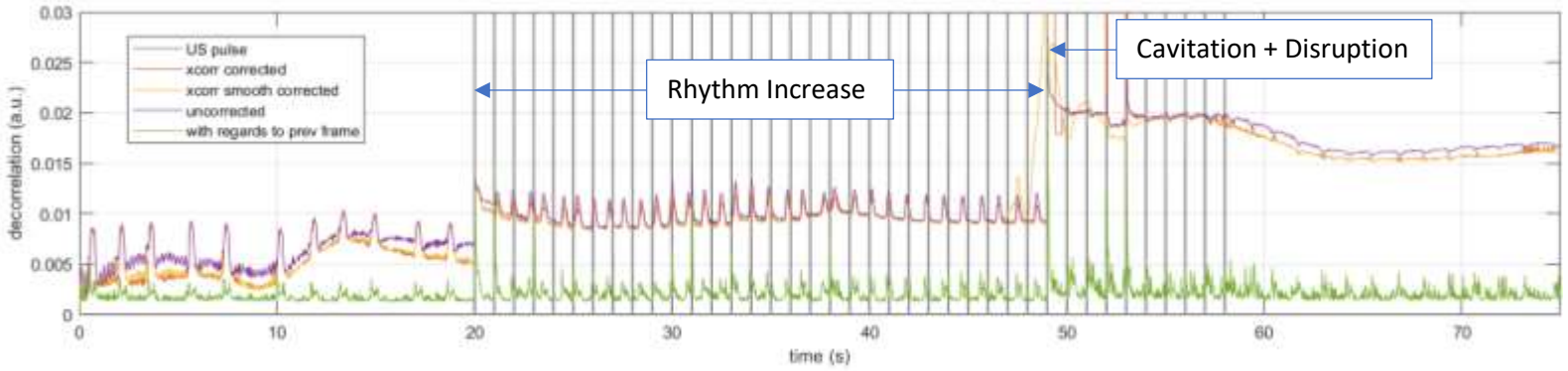

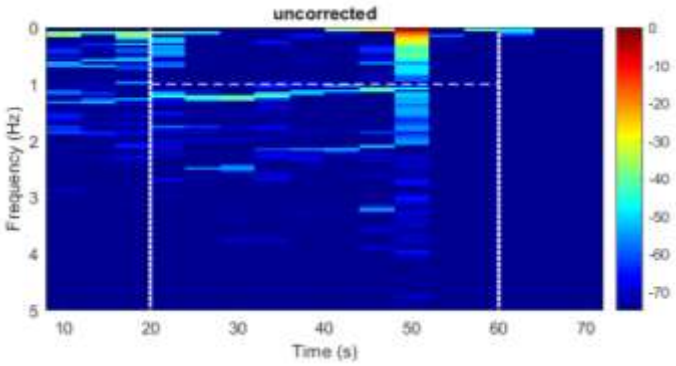

Figure 2.9: Movement plot and running Fourier plot of a tissue subjected to US pulses of 1 MHz and 1 ms long. Rhythm increased immediately at the start of sonication, though to a frequency slightly higher than the PRF. At 49s a cavitation occurs, causing a disruption of the tissue. Ultrasound pulses are shown as vertical gray lines in the movement plot. The start and end of the TUS are shown as vertical white dotted lines in the Fourier plot, and the horizontal line indicates the PRF.

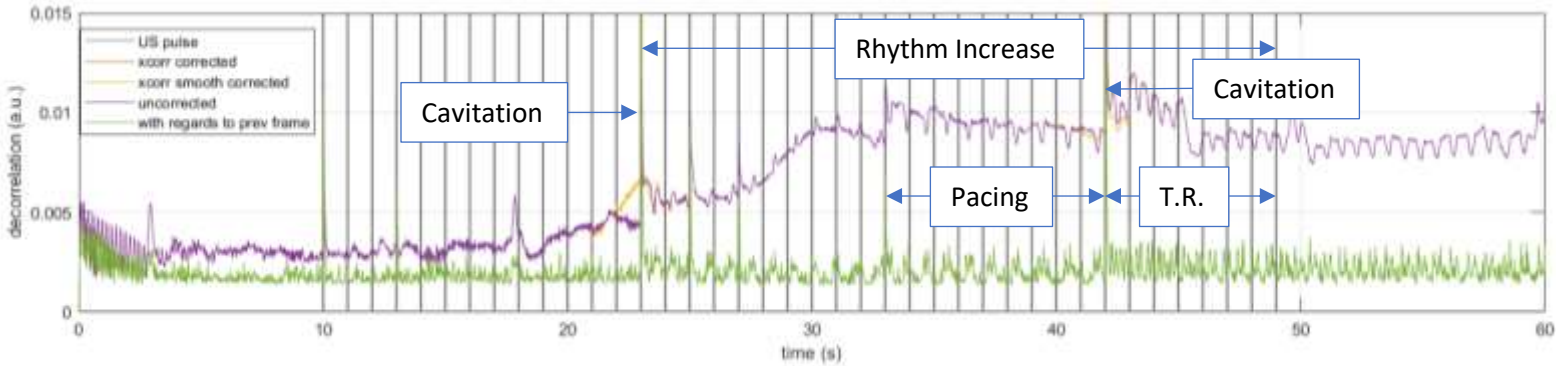

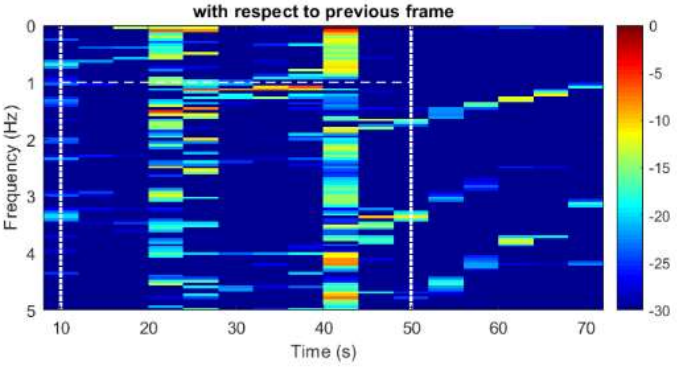

Figure 2.10: Movement plot and running Fourier plot of a tissue subjected to US pulses of 1 MHz and 0.5 ms long. Rhythm increased after a cavitation at 23s. Pacing is achieved between 33 and 42s. At 42s another cavitation occurs, followed by tachyrhythmia.

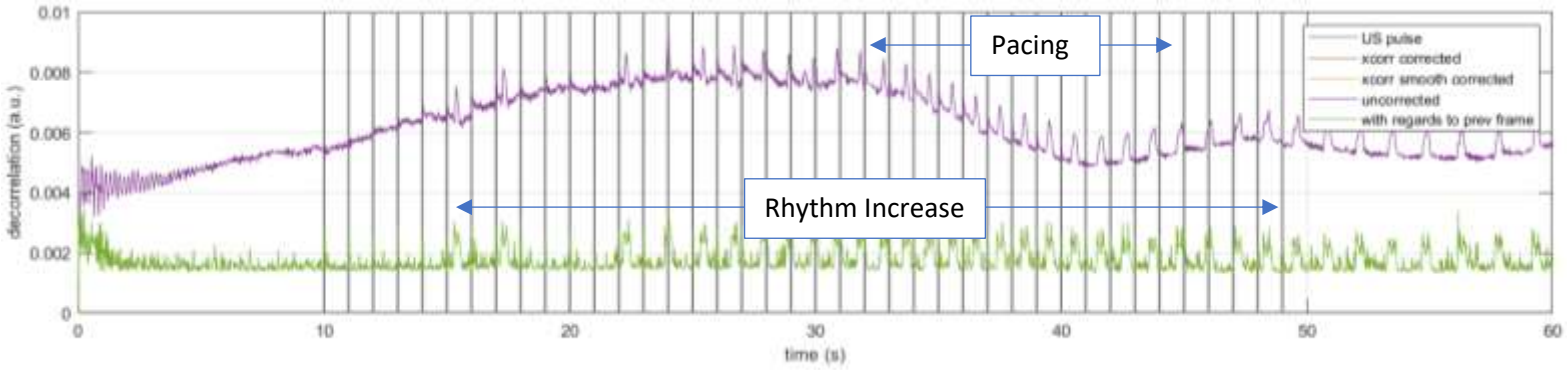

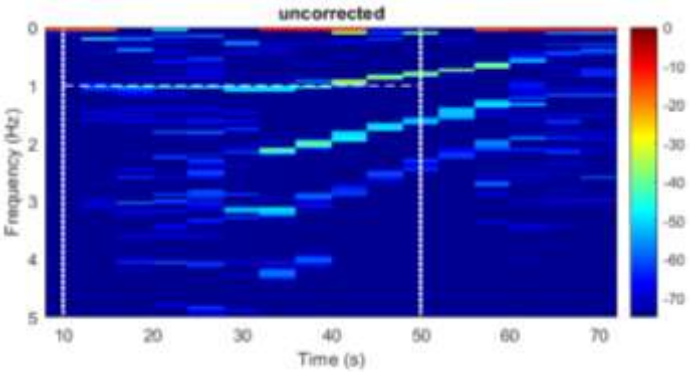

Figure 2.11: Movement plot and running Fourier plot of a tissue subjected to US pulses of 1.5 MHz and 0.7 ms long. The tissue displayed no automaticity prior to sonication. Pacing is achieved at about 32s until 45s, where the rhythm starts dropping again.

See appendix A for the complete oversight of the tested parameters and the number of biological and technical repeats. For all recordings, the occurrence of these events was collected. Any responses after a disruption were disregarded. Single contractions that occurred 'out of rhythm' were counted as 1xPRP and seen as a pacing event. Figure 2.12 displays the spread of total rhythm increase and total pacing duration of all usable recordings for 1.0 and 1.5 MHz ultrasound. While 0.5 and 0.7 MHz were tested, tissue response to these parameters, if any, was extremely limited, which caused these conditions to be abandoned early on in favour of the higher centre frequencies. Generally, rhythm increases were observed at the higher pulse durations for either frequency, albeit with great variation between measurements. Actual pacing was more rare than general rhythm increases, but similarly occurred at the higher pulse durations tested.

During the experiments the hypothesis arose that the automaticity of the tissues was an interfering factor for acoustic pacing. In order to investigate this, the difference between the PRF and automaticity frequency was compared to the duration of rhythm increase and pacing in figure 2.13. While the figure does not account for the pulse durations used in each experiment, it does indicate that there are more and longer periods of rhythm increase and pacing, if there is a larger difference between the PRF and the automaticity frequency.

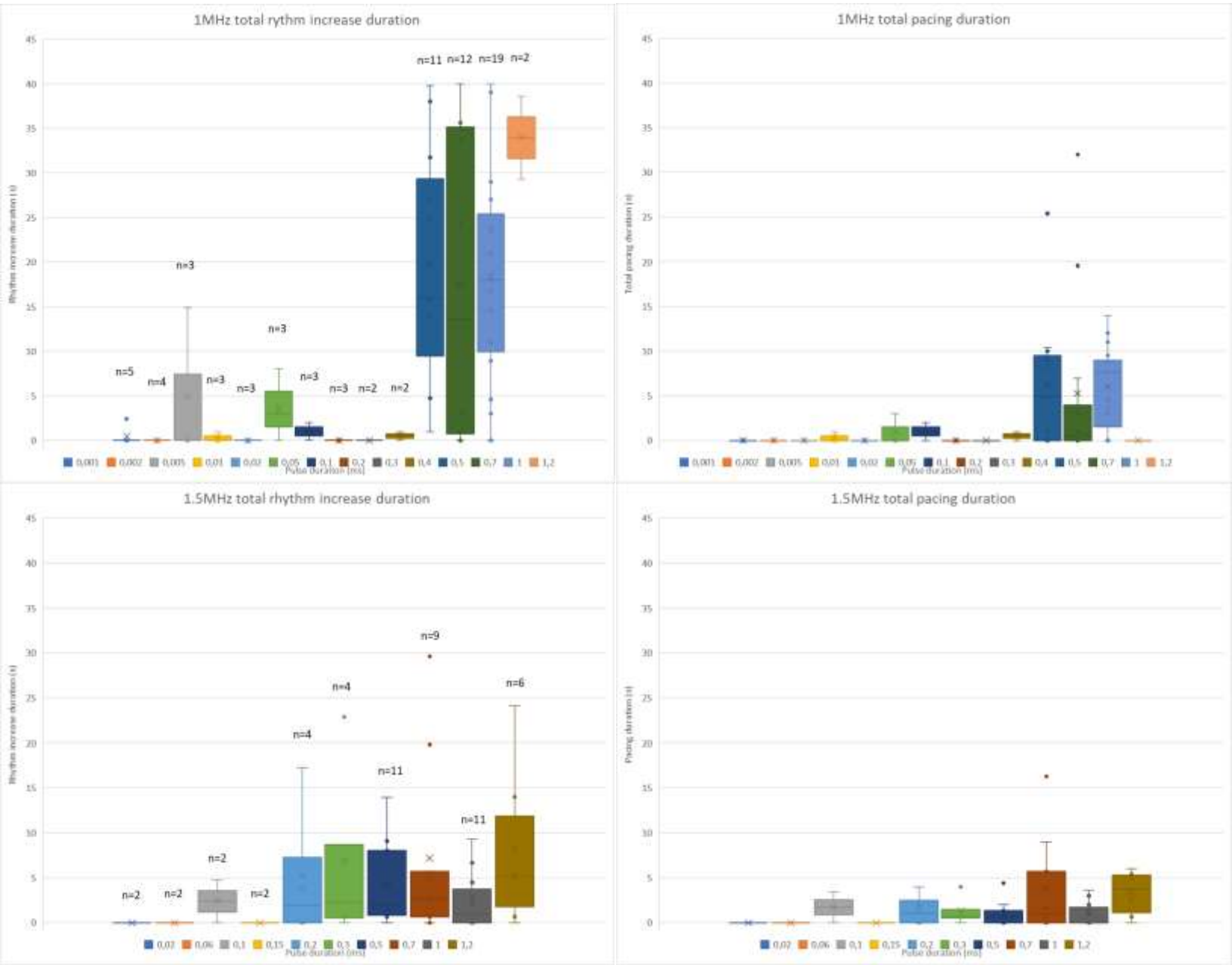

Figure 2.12: Total rhythm increase duration and total pacing duration of tissues subjected to 1 and 1.5 MHz ultrasound pulses. Sample size is indicated in the total rhythm increase plots.

The average amount of cavitations per recording is plotted in figure 2.14. Cavitations were of ambiguous benefit to the purpose of pacing. Rhythm changes could be elicited by cavitations, as shown in figure 2.10, but cavitations were also disruptive; if tissue disruptions occurred it they were always due to caviation events. As with the occurrence of rhythm increase and pacing, the number of cavitations per recording increased with pulse duration, though fewer cavitations were observed in 1.5MHz recordings compared to 1MHz recordings.

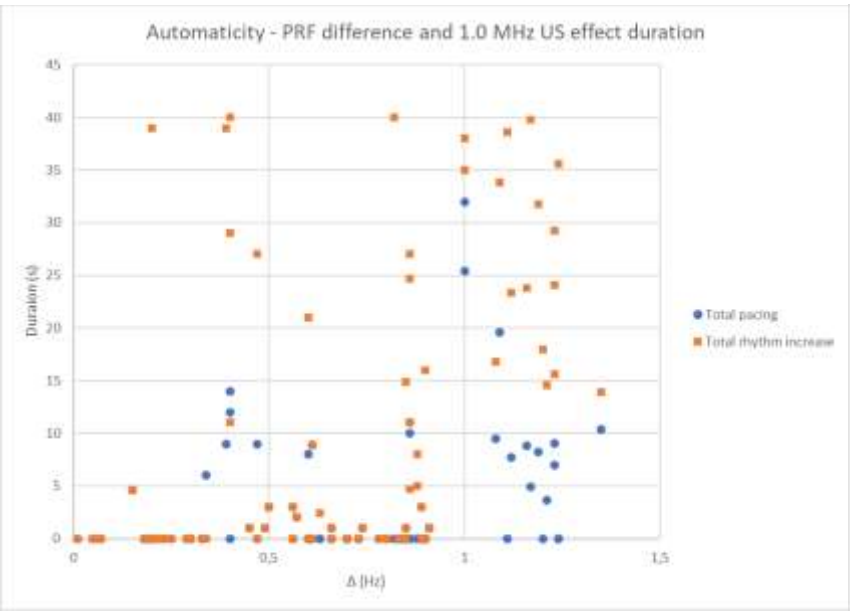

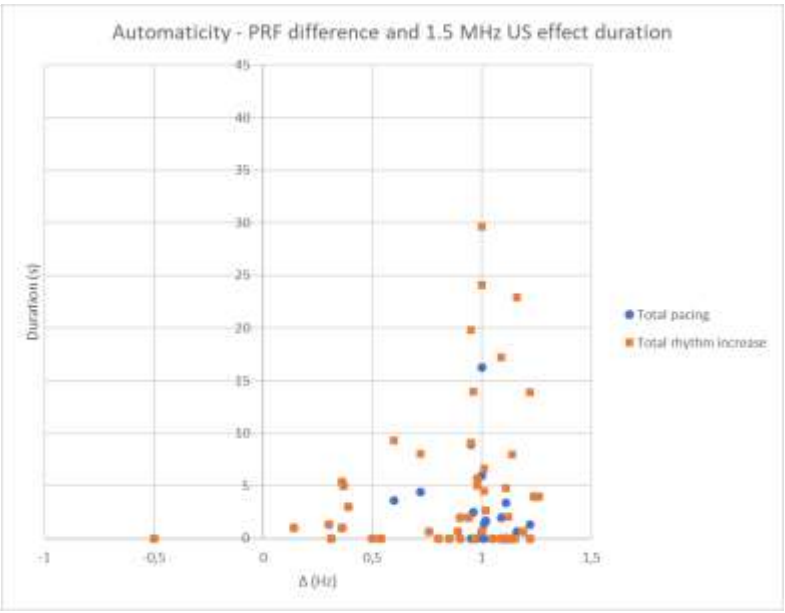

Figure 2.5: Relation between the total duration of rhythm increase or pacing and the difference between the PRF and automaticity frequency for 1 MHz (left) and 1.5 MHz ultrasound (right).

Tachyrhythmias were a rare occurrence, observed in six recordings out of a total of 151. See table 2.2 for the specifics of these observations. Due to the limited occurrence no clear correlations can be drawn between tachyrhythmias and US parameters or US timing.

Table 2.2: Occurrence of tachyrhythmia

f_c (MHz)	t_p (ms)	n_{tachy} (n_{total})
0,7	1,0	1 (4)
1,0	0,5	2 (11)
	0,7	2 (12)
	1,0	1 (19)

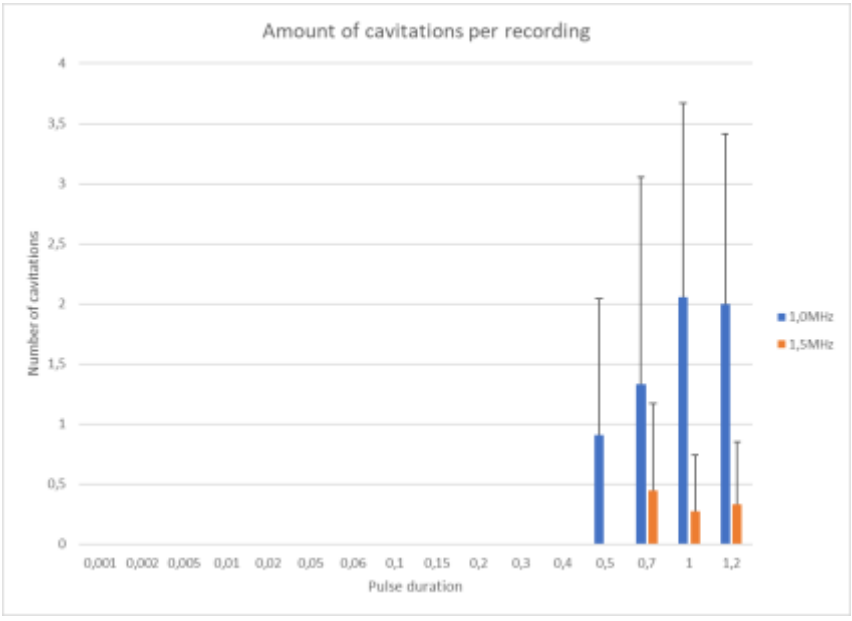

Figure 2.14: average amount of cavitations per recording. Error bars indicate standard deviation

Acoustic pacing of cardiac tissue – Discussion

Unfortunately, no definitive method of acoustic pacing has been found. However, the method provided here did sometimes allow for ephemeral periods of pacing or more general rhythm alterations. Such events were more reliably achieved using pulse durations of 0.5ms or more at centre frequencies of 1 or 1.5 MHz. It should be noted that this data is subject to a certain level of bias due to the low amount of repeats at the other parameters and the apparent high variation of response of the tissues. Furthermore, due to variations in the quality of the processed data the data analysis was performed manually, and as such, is subject to a certain degree of subjectivity. Due to time constraints this analysis was only performed by one person. Ideally, all experimental parameters are to be repeated for the same amount of times for a more reliable data set. Existing literature suggests that acoustic pressure rather than centre frequency is a determining factor in eliciting contractions through acoustic stimulation. As with the setup used here, the acoustic pressure increases with the centre frequency (table 2.1), the data here does not refute these findings. Further experiments where centre frequency and acoustic pressure are varied independently from one another would be useful for confirmation.

It is unclear why such a large variation exists in tissue response to the same stimulus. Automaticity appears to be part of this conundrum. If an ultrasound pulse hits tissue already undergoing an automatic contraction cycle, it cannot elicit another contraction. There is a limited time window of vulnerability to US stimulation in between the automatic pulses. Thus for a smaller difference between the automaticity frequency and the US PRF, it's less likely for a pulse to be able to induce contraction. Furthermore if this difference is really small, automaticity and pacing will become indistinguishable, which means pacing simply could not be confirmed with the current method of analysis. Further complicating this is the fact that various automaticity origins and propagation pathways exist in one tissue. These pathways are not entirely separate and might interfere with one another.

A certain degree of change in whether or not an US pulse was able to elicit a contraction was observed by *Marquet et al. (2016)* when attempting to acoustically pace an entire *ex vivo* pig heart. They increased this change by increasing the acoustic pressure and pulse duration and accounted for automaticity by timing pulses by ECG readout. Unfortunately, as *in vitro* tissues as used here are significantly less robust than an entire heart, this is simply not possible for *in vitro* applications. If every pulse only has a certain chance to cause contraction, it explains the observed periods of rhythm increase that fall short of reaching the PRF in frequency. The parameters that (somewhat) more reliably elicited a tissue response, also led to an increase in cavitations. Repeat experiments using high-speed cameras could elucidate whether the observed phenomenon here referred to as 'cavitation', are indeed inertial cavitations as described in the theory section. As stated before, the 'cavitations' observed could start frequency changes. If these events are indeed intertial cavitations, the rhythm change is likely caused by the pressure spikes caused by them. Such a spike might cause any vulnerable cells, even outside the focal area, to contract simultaneously. This would synchronize the various automaticity pathways, making further pacing easier. While these events do often elicit changes in the contraction rhythm, they are also disruptive: at times causing the tissue to detach from the membrane and generally disturbing the recording and complicating the data processing and analysis. Non-inertial cavitation could be used to amplify the US effects without risking the structural integrity of the tissues. This has already been shown by *Ibsen et al. (2015)* who used microbubbles to amplify the effect of low power US on mechanosensitive TRP4 channels through non-inertial cavitation.

Marquet et al. also observed that tachyrhythmia could be initiated by firing a single pulse during the refractory period of the heart. This could explain the tachyrhythmias observed here. This is difficult to confirm however, as the current method records movement, not the electrical cycle. Given the more random structure of the tissues used here compared to the *ex vivo* heart used by Marquet et al., another explanation could be that the US stimulates a portion of the tissue vulnerable to re-entry.

It would benefit the efforts for acoustic pacing if a method was employed to monitor the contraction cycle more directly, i.e. monitoring the membrane potential of the cells in the focal area. The easiest way this could probably be achieved would be through a voltage sensitive fluorescent dye. If the timing of the pulses was coupled to the fluorescence readout from the tissues, this setup would allow stimulation of the tissues exactly after repolarization. It would also improve the readout from the setup. The current method of measuring contractions, through digital detection of motion in video recordings, is extremely sensitive to disturbances. The setup was not placed on an anti-vibration table, causing disturbances in the recording by simply pressing the start button. Furthermore the analysis of several recordings was ruined by the presence of moving shadows from out-of-focus debris. Having a more direct way of monitoring contractions might help to alleviate these issues.

Several further improvements could be made to the setup used here. First and foremost, for the purpose of pacing *in vitro* tissues, the setup should be in a sterile environment. The medium reservoir used is rather large, requiring about 700 ml of medium to be properly filled. To properly heat the medium, a magnetic stirrer is used, this however does cause bubbles and debris to float around, possibly interfering with the ultrasound pulses. The medium is further exposed to the environment, which could lead to further contamination with dust or other particles. A smaller, enclosed reservoir, that could be heated without the need for stirring would therefore be much more convenient.

Conclusion

In conclusion, this thesis documents the research performed in two separate projects within the overarching context of *in vitro* modelling of cardiac arrhythmias. The existing method on developing and optimizing a method for modelling re-entry by reflection using PDMS shapes has been expanded upon with an optimal choice in protein coating and a redesign of the shapes themselves, allowing for longer term culture. Initial readout tests with calcium imaging and voltage optical mapping were promising, and save for some minor adjustments, the model seems suitable for investigating arrhythmias.

Initial tests with acoustic pacing have been promising. Various reactions of tissues of cardiac cells were observed, including the desired pacing, tachyrhythmia and more general changes in contraction rhythm and rate. The possibility to pace through ultrasound is apparent, though further research is a necessity to elucidate the mechanisms at play and to reduce the high variability in results observed.

Thus, these reports contribute to the ultimate goal of advanced *in vitro* models of cardiac disease for more efficient development of (personalized) treatments.

References

Geometrically constrained tissue culture

Allessie, M. A., Bonke, F. I., & Schopman, F. J. (1977). Circus movement in rabbit atrial muscle as a mechanism of tachycardia. III. The "leading circle" concept: A new model of circus movement in cardiac tissue without the involvement of an anatomical obstacle. *Circulation Research, 41*(1), 9-18. doi:10.1161/01.res.41.1.9

Alonso, A., & Larriva, A. P. A. D. (2016). Atrial Fibrillation, Cognitive Decline and Dementia. European Cardiology Review, 11(1), 49–53. doi: 10.15420/ecr.2016:13:2

Bajpai, A., Savelieva, I., & Camm, A. J. (2007). Epidemiology and economic burden of atrial fibrillation. *US Cardiology*, *4*(1), 14-17.

Beavers, D. L., Wang, W., Ather, S., Voigt, N., Garbino, A., Dixit, S. S., . . . Wehrens, X. H. (2013). Mutation E169K in Junctophilin-2 Causes Atrial Fibrillation Due to Impaired RyR2 Stabilization. Journal of the American

Brandão, K. O., Tabel, V. A., Atsma, D. E., Mummery, C. L., & Davis, R. P. (2017). Human pluripotent stem cell models of cardiac disease: from mechanisms to therapies. Disease Models & Mechanisms, 10(9), 1039–1059. doi: 10.1242/dmm.030320

Chugh, S. S., Havmoeller, R., Narayanan, K., Singh, D., Rienstra, M., Benjamin, E. J., . . . Murray, C. J. (2013). Worldwide Epidemiology of Atrial Fibrillation: A Global Burden of Disease 2010 Study. Circulation, 129(8), 837-847. doi:10.1161/circulationaha.113.005119

Chugh, S. S., Roth, G. A., Gillum, R. F., & Mensah, G. A. (2014). Global Burden of Atrial Fibrillation in Developed and Developing Nations. Global Heart, 9(1), 113-119. doi:10.1016/j.gheart.2014.01.004

Ciaccio, E. J., Coromilas, J., Wit, A. L., Peters, N. S., & Garan, H. (2018). Source-Sink Mismatch Causing Functional Conduction Block in Re-Entrant Ventricular Tachycardia. JACC: Clinical Electrophysiology, 4(1), 1–16. doi: 10.1016/j.jacep.2017.08.019

Clauss, S., Bleyer, C., Schüttler, D., Tomsits, P., Renner, S., Klymiuk, N., … Kääb, S. (2019). Animal models of arrhythmia: classic electrophysiology to genetically modified large animals. Nature Reviews Cardiology, 16(8), 457–475. doi: 10.1038/s41569-019-0179-0

Dobrev, D., & Wehrens, X. H. (2017). Calcium-mediated cellular triggered activity in atrial fibrillation. *The Journal of Physiology, 595*(12), 4001-4008. doi:10.1113/jp273048

Dzeshka, M. S., Lip, G. Y., Snezhitskiy, V., & Shantsila, E. (2015). Cardiac Fibrosis in Patients With Atrial Fibrillation. *Journal of the American College of Cardiology, 66*(8), 943-959. doi:10.1016/j.jacc.2015.06.1313

Fast, V. G., & Kléber, A. G. (1997). Role of wavefront curvature in propagation of cardiac impulse. Cardiovascular Research, 33(2), 258-271. doi:10.1016/s0008-6363(96)00216-7

Flaker, G. C., Belew, K., Beckman, K., Vidaillet, H., Kron, J., Safford, R., . . . Barrell, P. (2005). Asymptomatic atrial fibrillation: Demographic features and prognostic information from the Atrial Fibrillation Follow-up Investigation of Rhythm Management (AFFIRM) study. American Heart Journal, 149(4), 657-663. doi:10.1016/j.ahj.2004.06.032

Gonçalves, A. (2018) Atrial Fibrillation Modelling: Report on Genetic engineering & Geometrically-constrained culture modelling approaches for AF. Unpublished manuscript.

Heijman, J., Voigt, N., Wehrens, X. H., & Dobrev, D. (2014). Calcium dysregulation in atrial fibrillation: The role of CaMKII. Frontiers in Pharmacology, 5. doi:10.3389/fphar.2014.00030

Kucera, J. P., Kleber, A. G., & Rohr, S. (1998). Slow Conduction in Cardiac Tissue, II : Effects of Branching Tissue Geometry. Circulation Research, 83(8), 795-805. doi:10.1161/01.res.83.8.795

Lumen Boundless Anatomy and Physiology. (n.d.). Cardiac Muscle Tissue. Retrieved March 4, 2020, from https://courses.lumenlearning.com/boundless-ap/chapter/cardiac-muscle-tissue/

Nattel, S. (2002). New ideas about atrial fibrillation 50 years on. *Nature, 415*(6868), 219-226. doi:10.1038/415219a

Nattel, S., & Harada, M. (2014). Atrial Remodeling and Atrial Fibrillation. *Journal of the American College of Cardiology, 63*(22), 2335-2345. doi:10.1016/j.jacc.2014.02.555

NIH. (n.d.) Arrhythmia. Retrieved December 31, 2019, from https://www.nhlbi.nih.gov/health-topics/arrhythmia.

Pandit, S. V., & Jalife, J. (2013). Rotors and the Dynamics of Cardiac Fibrillation. *Circulation Research, 112*(5), 849-862. doi:10.1161/circresaha.111.300158

Park, M., & Yoon, Y.-S. (2018). Cardiac Regeneration with Human Pluripotent Stem Cell-Derived Cardiomyocytes. Korean Circulation Journal, 48(11), 974. doi: 10.4070/kcj.2018.0312

Pellman, J., Lyon, R. C., & Sheikh, F. (2010). Extracellular matrix remodeling in atrial fibrosis: Mechanisms and implications in atrial fibrillation. *Journal of Molecular and Cellular Cardiology, 48*(3), 461-467. doi:10.1016/j.yjmcc.2009.09.001

Pellman, J., & Sheikh, F. (2015). Atrial Fibrillation: Mechanisms, Therapeutics, and Future Directions. *Comprehensive Physiology,* 649-665. doi:10.1002/cphy.c140047

Priest, B. T., & Mcdermott, J. S. (2015). Cardiac ion channels. Channels, 9(6), 352-359. doi:10.1080/19336950.2015.1076597

Russo, I., & Frangogiannis, N. G. (2016). Diabetes-associated cardiac fibrosis: Cellular effectors, molecular mechanisms and therapeutic opportunities. *Journal of Molecular and Cellular Cardiology, 90*, 84-93. doi:10.1016/j.yjmcc.2015.12.011

Schotten, U., Verheule, S., Kirchhof, P., & Goette, A. (2011). Pathophysiological Mechanisms of Atrial Fibrillation: A Translational Appraisal. *Physiological Reviews, 91*(1), 265-325. doi:10.1152/physrev.00031.2009

Schwach, V., & Passier, R. (2016). Generation and purification of human stem cell-derived cardiomyocytes. Differentiation, 91(4-5), 126–138. doi: 10.1016/j.diff.2016.01.001

Voigt, N., Heijman, J., Wang, Q., Chiang, D. Y., Li, N., Karck, M., . . . Dobrev, D. (2013). Cellular and Molecular Mechanisms of Atrial Arrhythmogenesis in Patients With Paroxysmal Atrial Fibrillation. *Circulation, 129*(2), 145-156. doi:10.1161/circulationaha.113.006641

Voigt, N., Li, N., Wang, Q., Wang, W., Trafford, A. W., Abu-Taha, I., . . . Dobrev, D. (2012). Enhanced Sarcoplasmic Reticulum Ca2 Leak and Increased Na -Ca2 Exchanger Function Underlie Delayed Afterdepolarizations in Patients With Chronic Atrial Fibrillation. *Circulation, 125*(17), 2059-2070. doi:10.1161/circulationaha.111.067306

Waks, J. W., & Josephson, M. E. (2014). Mechanisms of Atrial Fibrillation – Reentry, Rotors and Reality. Arrhythmia & Electrophysiology Review, 3(2), 90. doi:10.15420/aer.2014.3.2.90

Yang, F., Tiano, J., Mittal, S., Turakhia, M., Jacobowitz, I., & Greenberg, Y. (2017). Towards a Mechanistic Understanding and Treatment of a Progressive Disease: Atrial Fibrillation. *Journal of Atrial Fibrillation, 10*(3). doi:10.4022/jafib.1627

Youn, J., Zhang, J., Zhang, Y., Chen, H., Liu, D., Ping, P., . . . Cai, H. (2013). Oxidative stress in atrial fibrillation: An emerging role of NADPH oxidase. *Journal of Molecular and Cellular Cardiology, 62*, 72-79. doi:10.1016/j.yjmcc.2013.04.019

Zhou, X., Bueno-Orovio, A., & Rodriguez, B. (2018). In silico evaluation of arrhythmia. Current Opinion in Physiology, 1, 95–103. doi: 10.1016/j.cophys.2017.11.003

Acoustic Pacing

Biesheuvel, P. M., & Dykstra, J. E. (2018, September 9). The difference between Faradaic and Nonfaradaic processes in Electrochemistry. Retrieved January 6, 2020, from https://arxiv.org/abs/1809.02930.

Coiado, O. C., & Obrien, W. D. (2014). The role of the duty factor in ultrasound-mediated cardiac stimulation. *The Journal of the Acoustical Society of America, 136*(3). doi:10.1121/1.4893332

Dalecki, D., Keller, B. B., Raeman, C. H., & Carstensen, E. L. (1993). Effects of pulsed ultrasound on the frog heart: I. Thresholds for changes in cardiac rhythm and aortic pressure. Ultrasound in Medicine & Biology, 19(5), 385–390. doi: 10.1016/0301-5629(93)90057-u

Dalecki, D., Raeman, C. H., Child, S. Z., & Carstensen, E. L. (1997). Effects of pulsed ultrasound on the frog heart: III. The radiation force mechanism. Ultrasound in Medicine & Biology, 23(2), 275–285. doi: 10.1016/s0301-5629(96)00209-8

Dwenger, M., Kowalski, W. J., Ye, F., Yuan, F., Tinney, J. P., Setozaki, S., … Keller, B. B. (2019). Chronic optical pacing conditioning of h-iPSC engineered cardiac tissues. Journal of Tissue Engineering, 10, 204173141984174. doi: 10.1177/2041731419841748

Food and Drug Administration, Center for Devices and Radiological Health (2008) *Information for Manufacturers Seeking Marketing Clearance of Diagnostic Ultrasound Systems and Transducers*. Retrieved from: https://www.fda.gov/downloads/MedicalDevices/DeviceRegulationandGuidance/GuidanceDocuments/UCM070911.pdf

Gibbs, V., Cole, D., & Sassano, A. (2009). *Ultrasound physics and technology: How, why and when*. Edinburgh: Churchill Livingstone/Elsevier.

Hoskins, P., Martin, K., & Thrush, A. (2010). Diagnostic ultrasound: Physics and equipment. Cambridge: Cambridge University Press.

Ibsen, S., Tong, A., Schutt, C., Esener, S., & Chalasani, S. H. (2015). Sonogenetics is a non-invasive approach to activating neurons in Caenorhabditis elegans. *Nature Communications, 6*(1). doi:10.1038/ncomms9264

Izadifar, Z., Babyn, P., & Chapman, D. (2017). Mechanical and Biological Effects of Ultrasound: A Review of Present Knowledge. *Ultrasound in Medicine & Biology, 43*(6), 1085-1104. doi:10.1016/j.ultrasmedbio.2017.01.023

Jiang, C., Li, H. T., Zhou, Y. M., Wang, X., Wang, L., & Liu, Z. Q. (2017). Cardiac optogenetics: a novel approach to cardiovascular disease therapy. EP Europace. doi: 10.1093/europace/eux345

Kim, J. J., Yang, L., Lin, B., Zhu, X., Sun, B., Kaplan, A. D., … Salama, G. (2015). Mechanism of automaticity in cardiomyocytes derived from human induced pluripotent stem cells. Journal of Molecular and Cellular Cardiology, 81, 81–93. doi: 10.1016/j.yjmcc.2015.01.013

Kubanek, J., Shi, J., Marsh, J., Chen, D., Deng, C., & Cui, J. (2016). Ultrasound modulates ion channel currents. *Scientific Reports, 6*(1). doi:10.1038/srep24170

Marquet, F., Bour, P., Vaillant, F., Amraoui, S., Dubois, R., Ritter, P., … Quesson, B. (2016). Non-invasive cardiac pacing with image-guided focused ultrasound. Scientific Reports, 6(1). doi: 10.1038/srep36534

Merrill, D. R., Bikson, M., & Jefferys, J. G. (2005). Electrical stimulation of excitable tissue: design of efficacious and safe protocols. Journal of Neuroscience Methods, 141(2), 171–198. doi: 10.1016/j.jneumeth.2004.10.020

Miller, M. W., Miller, D. L., & Brayman, A. A. (1996). A review of in vitro bioeffects of inertial ultrasonic cavitation from a mechanistic perspective. *Ultrasound in Medicine & Biology, 22*(9), 1131-1154. doi:10.1016/s0301-5629(96)00089-0

Nelson, T. R., Fowlkes, J. B., Abramowicz, J. S., & Church, C. C. (2009). Ultrasound Biosafety Considerations for the Practicing Sonographer and Sonologist. *Journal of Ultrasound in Medicine, 28*(2), 139-150. doi:10.7863/jum.2009.28.2.139

Palmeri, M., Sharma, A., Bouchard, R., Nightingale, R., & Nightingale, K. (2005). A finite-element method model of soft tissue response to impulsive acoustic radiation force. IEEE Transactions on Ultrasonics, Ferroelectrics and Frequency Control, 52(10), 1699–1712. doi: 10.1109/tuffc.2005.1561624Prince, J. L., & Links, J. M. (2015). Medical imaging: Signals and systems. Upper Saddle River, NJ: Pearson Education.

Tandon, N., Cannizzaro, C., Chao, P. H. G., Maidhof, R., Marsano, A., Au, H. T. H., … Vunjak-Novakovic, G. (2009). Electrical stimulation systems for cardiac tissue engineering. Nature Protocols, 4(2), 155–173. doi: 10.1038/nprot.2008.183

Williams, J., & Entcheva, E. (2015). Optogenetic versus Electrical Stimulation of Human Cardiomyocytes: Modeling Insights. *Biophysical Journal, 108*(8), 1934-1945. doi:10.1016/j.bpj.2015.03.032

Appendix A – Data analysis code

Provided here is the full Matlab code used to analyse the ultrasound recordings. A single US measurement will result in an image sequence folder containing .tif files and a corresponding .xiseq file. Ensure that the image sequence folders and corresponding .xiseq files are in the same folder. Use CONSTRUCTION_AVIS_FROM_TIFS.M to process the raw image sequences to .avi movies. Place all the video files you want to analyse in the same folder as their corresponding .xiseq files. Ensure that IMPORTFILE_XIMEA.M, SMOTH_DATA.M and ANALYSIS_V4.M are placed in the same folder, and run the latter script. Analysis will take about 30 to 60 min per video, depending on video length.

CONSTRUCTION_AVIS_FROM_TIFS.M

```
%% This file converts .tiff files to 1 .AVI file
clc; clear all; close all;

%% Step 1: select all xiseq files (=same name as folders) that need to be analyzed
% ask for the files
% Select as many xiseq files if you want, but only in the same folder!!
[all_files, path] = uigetfile('*.xiseq', 'multiselect', 'on');
tic
%% Step 2: Find the folder for each measurement and find the folder
% Loop for all files
for jj=1:length(all_files)
    % Add a folder for the results
    % Find all the slashes
    pobar = strfind(path,'\');
    % Construct the correct foldername
    folder=join([path(1:pobar(end)) all_files(jj)]);
    folder{1,1}(pobar(end)+1)='';
    folder{1,1}(end-5:end)='';
    folder=join([folder '_files']);
    folder{1,1}(end-6)='';
    % Open the cell
    yourfolder=folder{1,1};

    % Find the amount of frames; number of tif files in 'yourfolder'
    a = dir(fullfile(yourfolder, '*.tif'));
    framenumbers=length(a);

    % Define the video
    videoname=all_files(jj);
    videoname=videoname{1,1}(1:end-6);
    v = VideoWriter([path videoname, '.avi'],'Motion JPEG AVI');
    v.FrameRate=50;
    open(v);

    % Add all framenumbers to the video
    for jk=1:framenumbers
        framename=char(['000000000', num2str(jk)]);
        framename=framename(end-5:end);
        A=imread([yourfolder '\' framename '.tif']);
        writeVideo(v,A);
    end
    close(v);
end
toc
```

ANALYSIS.M

```
%% Analysis of movies of (20x) cardiomyocytes
% Goal: to be able to know if contraction takes place
%% Basics and selection of the movie to analyze
% Basics for starting a new document
clear all
clc
close all

% ask for the movie(s)
[all_movies, pa] = uigetfile('*.avi', 'multiselect', 'on');

% Add a folder for the results
pobar = strfind(pa,'\');
paresult=[pa(1:pobar(end-1)) 'Results_V4']; % V1.0 is for the version of the script
if ~isdir(paresult)
    mkdir(paresult);
end
%%
fps=50;

% Analyse all the videos one by one
for ii=1:length(all_movies)
    close all
    % Declare fps again since a parfor loop will clear it at the beginning
    % at each iteration.
    fps=50;

    % select the movie for analysis and determine some parameters
    fi=all_movies(ii);
    mov = VideoReader([pa, fi{1,1}]);
    framenumbers=mov.NumberOfFrame;

    % Automatic implementation of PRF information etc.
    PRF_index=strfind(fi,'PRF');
    PRF=str2num(fi{1,1}((PRF_index{1,1})+3:(PRF_index{1,1})+5));
    WT_index=strfind(fi,'WT');
    waitingtime=str2num(fi{1,1}((WT_index{1,1})+2:(WT_index{1,1})+3));
    TUS_index=strfind(fi,'TUS');
    UStime=str2num(fi{1,1}((TUS_index{1,1})+3:(TUS_index{1,1})+4));

    % Contruct a time array based on the timefile if xiseq is saved
    name_info = [pa fi{1,1}(1:end-4) '.xiseq'];
    if isfile(name_info)
        EB1control = importfile_ximea(name_info);

        % Get the timestamp line (strings)
        timestamp_line = EB1control(:,2 );
        temp = timestamp_line{100}{1};

        % If the 'timestamp line' consists of frame numbers, choose the other
        % column for timestamps (imageJ adds them randomly in column 2 or 3)
        if ~contains(temp,'timestamp')
            timestamp_line = EB1control(:,3);
        end

        % a time array is created, based on the timestamp of the xiseq file
        time = [];
        for i = 1:length(timestamp_line)
            temp = timestamp_line{i}{1};
            if contains(temp,'timestamp')
                po = strfind(temp,'"');
```

```
            time_char = temp(po(1)+1:po(2)-1);
            time(end+1) = str2double(time_char);
        end
    end

    % Let the time start at 0
    time=time-time(1);
    time(time<0) = time(time<0)+2^32;
    time = time.*1e-6; % time is in seconds
    mean_Ts=time(end)/length(time);

    % Insert a signal that displays the US pulse
    US_pulse=zeros(length(time),1);
    if UStime~=0
        US_pulse(find(time >= waitingtime,1))=1;
        US_timing=[0:1/PRF:UStime-0.2];
        for jj=1:length(US_timing)
            US_pulse(find(time>= waitingtime+US_timing(jj),1))=1;
        end
    end

else
    % Instead of using the ximea file, use this 'ideal' time line
    starttime=0;
    fps=50;
    mean_Ts=1/fps;
    endtime=(framenumbers-1)*mean_Ts;
    time=[starttime:mean_Ts:endtime];

    % insert the US pulse line
    US_pulse=zeros(length(time),1);
    if UStime~=0
        US_pulse(waitingtime*fps+1:fps/PRF:(waitingtime+UStime-1)*fps)=1;
    end
    % Ensure that US_pulse has same length as time
    US_pulse(length(time)+1:end)=[];
end
mean_fs=1/mean_Ts;

if length(time)>framenumbers
    time(framenumbers+1:end)=[];
    US_pulse(framenumbers+1:end)=[];
end

coresize = 0.25; % If you want to speed up, make this number smaller
imsize=size(read(mov,1)); % resize the frames
imsizered=coresize.*imsize(1:2);

% Preallocate arrays for saving resutls
deltav = zeros(2,framenumbers-1);
beat = zeros(1,framenumbers);
beat_xcorr_smooth = zeros(1,framenumbers);
beat_uncorrected = zeros(1,framenumbers);
var_prev_fr = zeros(1,framenumbers);
mean_control = zeros(1,framenumbers);

% Defining the first frame
frame1=read(mov,1);
Aref1=double(frame1(:,:,1)); % not sure if step is correct
Aref1red=imresize(Aref1,coresize);

% compare all other timeframes with the first one and the previous one
for i = 2:framenumbers
```

```
    % take the i frame
    framei=read(mov,i);
    frameiD=double(framei(:,:,1));
    Aired=imresize(frameiD,coresize);

    % Compare the i frame with the 0 frame via norm xcorr2
    X = normxcorr2(Aref1red,Aired); % this function takes a while!

    % Bicubic interpolation to obtain right size
    X_g=imresize(X,[2*imsize(1)+1,2*imsize(2)+1],'bicubic');
    maximum=max(X_g,[],'all');
    [r,c]=find(X_g==maximum);
    delta=[r-imsize(1)-1,c-imsize(2)-1];
    deltav(:,i-1) = delta;
end

% Show the delta v in both directions over time
time_short = time(1:end-1);

% Smooth the movement
[fitresult, ~] = smoth_data(time_short, deltav(1,:));
y1 = int16(fitresult(time_short));
[fitresult, ~] = smoth_data(time_short, deltav(2,:));
y2 = int16(fitresult(time_short));

Afi=Aref1;
for i=2:framenumbers
    delta=deltav(:,i-1);
    % Get the i'th frame
    framei2=read(mov,i);
    Atoti=double(framei2(:,:,1));

    % calculate diff between i'th frame and fist frame
    err_uncorrected = Atoti-Aref1;

    % calculate diff between i'th frame and the frame before
    err_prev_fr = Atoti-Afi;
    % initialization for normalisation
    numpix=size(err_uncorrected,1)*size(err_uncorrected,2);

    % Take the root mean square
    beat_uncorrected(i) = sqrt(sum(sum(err_uncorrected.^2)))/numpix;
    var_prev_fr(i) = sqrt(sum(sum(err_prev_fr.^2)))/numpix;

    % Initialization values
    Aicorr=Atoti;
    Aref_2corr=Aref1;

    % Delete the borders that are not in two subsequent frames;
    % The resulting values are location values, so one can compare
    % movement over time
    if delta(1)>0
        Aicorr(1:delta(1),:) = [];
        Aref_2corr(end-delta(1)+1:end,:) = [];
    elseif  delta(1)<0
        Aref_2corr(1:-delta(1),:) = [];
        Aicorr(end+delta(1)+1:end,:) = [];
    end

    % Delete the borders that are not in two subsequent frames
    if delta(2)>0
        Aicorr(:,1:delta(2)) = [];
        Aref_2corr(:,end-delta(2)+1:end) = [];
```

```
        elseif  delta(2)<0
            Aref_2corr(:,1:-delta(2)) = [];
            Aicorr(:,end+delta(2)+1:end) = [];
        end

        err = Aicorr-Aref_2corr;
        beat(i) = sqrt(sum(sum(err.^2)))/(size(err,1)*size(err,2));
        mean_control(i) = mean(Aicorr(:));

        Aicorr2=Atoti;
        Aref_2corr2=Aref1;
        if y1(i-1)>0
            Aicorr2(1:y1(i-1),:) = [];
            Aref_2corr2(end-y1(i-1)+1:end,:) = [];
        elseif  y1(i-1)<0
            Aref_2corr2(1:-y1(i-1),:) = [];
            Aicorr2(end+y1(i-1)+1:end,:) = [];
        end

        if y2(i-1)>0
            Aicorr2(:,1:y2(i-1)) = [];
            Aref_2corr2(:,end-y2(i-1)+1:end) = [];
        elseif  y2(i-1)<0
            Aref_2corr2(:,1:-y2(i-1)) = [];
            Aicorr2(:,end+y2(i-1)+1:end) = [];
        end
        err2 = Aicorr2-Aref_2corr2;
        beat_xcorr_smooth(i) = sqrt(sum(sum(err2.^2)))/(size(err2,1)*size(err2,2));

        % To start a new loop
        Afi=Atoti;
    end

    % Resulting location time diagram
    h20 = figure(20);

    plot(time_short,5*US_pulse(2:end), 'LineWidth', 2);

    hold all
    plot(time_short,deltav(1,:));
    plot(time_short,y1);
    plot(time_short,deltav(2,:));
    plot(time_short,y2);

    hold off
    grid on
    title([fi{1,1}(1:end-4)])
    legend('Location','northwest')
    legend('US pulse', 'position 1','position 1 smooth','position 2','position 2
smooth');
    xlabel('time (s)');
    ylabel('displacement (pix)');
    xlim([0 80])
    ylim([-20 20])

    % Save the figure
    name = [paresult '\' fi{1,1}(1:end-4) '_shift.fig'];
    saveas(h20,name,'fig');
    name = [paresult '\' fi{1,1}(1:end-4) '_shift.eps'];
    saveas(h20,name,'epsc');
    name = [paresult '\' fi{1,1}(1:end-4) '_shift.jpg'];
    saveas(h20,name,'jpg');
```

```
    % Short time fourier transform
    % parameters used in analysis
    npt=length(var_prev_fr);
    window=round(npt/8);
    noverlap=round(window*0.8);
    time=time-time(1);
    fs=1/mean_Ts;

    % Define the signal
    x1=beat-mean(beat);
    x2=beat_xcorr_smooth-mean(beat_xcorr_smooth); % This is the signal, consisting of
T/Ts samples
    x3=beat_uncorrected-mean(beat_uncorrected);
    x4=var_prev_fr-mean(var_prev_fr);

    [s1,f1,t1]=spectrogram(x1,hamming(window),noverlap,[],fs);
    [s2,f2,t2]=spectrogram(x2,hamming(window),noverlap,[],fs);
    [s3,f3,t3]=spectrogram(x3,hamming(window),noverlap,[],fs);
    [s4,f4,t4]=spectrogram(x4,hamming(window),noverlap,[],fs);

    h60 = figure(60);
    subplot(2,2,1)
    imagesc(t1,f1,log10(abs(s1)./max(max(abs(s1)))));
    xlabel('Time (s)')
    ylabel('Frequency (Hz)')
    title('xcorr corrected')
    c=colorbar;
    ylabel(c,'Amplitude (a.u.)');
    colorbar
    colormap hot
    caxis([-6 0])

    subplot(2,2,2)
    imagesc(t2,f2,log10(abs(s2)./max(max(abs(s2)))));
    xlabel('Time (s)')
    ylabel('Frequency (Hz)')
    title('xcorr smooth corrected')
    c=colorbar;
    ylabel(c,'Amplitude (a.u.)');
    colorbar
    colormap hot
    caxis([-6 0])

    subplot(2,2,3)
    imagesc(t3,f3,log10(abs(s3)./max(max(abs(s3)))));
    xlabel('Time (s)')
    ylabel('Frequency (Hz)')
    title('uncorrected')
    c=colorbar;
    ylabel(c,'Amplitude (a.u.)');
    colorbar
    colormap hot
    caxis([-6 0])

    subplot(2,2,4)
    imagesc(t4,f4,log10(abs(s4)./max(max(abs(s4)))));
    xlabel('Time (s)')
    ylabel('Frequency (Hz)')
    title('with respect to previous frame')
    c=colorbar;
    ylabel(c,'Amplitude (a.u.)');
    colorbar
    colormap hot
```

```
    caxis([-6 0])

    % Total figure title
    sgtitle([fi{1,1}(1:end-4)])

    % Save the spectograms
    name = [paresult '\' fi{1,1}(1:end-4) '_cell_beat_runningfourier.fig'];
    saveas(h60,name,'fig');
    name = [paresult '\' fi{1,1}(1:end-4) '_cell_beat_runningfourier.eps'];
    saveas(h60,name,'epsc');
    name = [paresult '\' fi{1,1}(1:end-4) '_cell_beat_runningfourier.jpg'];
    saveas(h60,name,'jpg');

        % above 12 Hz filtering if one wants to;
        fcutoff=7; % Continuous cut-off frequency in Hz
        Ts=mean_Ts;
        fcutoff_normalized=2*Ts*fcutoff; % normalized cutoff freq
        [lp_B,lp_A]=butter(2,fcutoff_normalized);
        beat=filter(lp_B,lp_A,beat);
        beat_xcorr_smooth=filter(lp_B,lp_A,beat_xcorr_smooth);
        beat_uncorrected=filter(lp_B,lp_A,beat_uncorrected);
        var_prev_fr=filter(lp_B,lp_A,var_prev_fr);

    % Display the result in figures
    h30 = figure(30);
    subplot(2,1,1);
    plot(time,US_pulse*0.15, 'LineWidth', 2);
    hold on
    plot(time,beat);
    plot(time,beat_xcorr_smooth);
    plot(time,beat_uncorrected);
    plot(time,var_prev_fr);
    hold off
    xlabel('time (s)');
    ylabel('decorrelation (a.u.)');
    grid on
    legend('US pulse', 'xcorr corrected','xcorr smooth corrected','uncorrected','with
regards to prev frame');
    xlim([0 80])
    ylim([0 0.15])

    mean_control(1) = mean_control(2);
    mean_control=mean_control/mean(mean_control);

    subplot(2,1,2);
    plot(time,US_pulse*2, 'LineWidth', 2);
    hold on
    plot(time,mean_control);
    hold off
    xlabel('Time (s)');
    ylabel('Frame average (light_intensity)');
    grid on
    xlim([0 80])
    ylim([0.80 1.80])
    sgtitle([fi{1,1}(1:end-4)])

    % Save the resulting figures to images
    name = [paresult '\' fi{1,1}(1:end-4) '_cell_beat.fig'];
    saveas(h30,name,'fig');
    name = [paresult '\' fi{1,1}(1:end-4) '_cell_beat.eps'];
    saveas(h30,name,'epsc');
    name = [paresult '\' fi{1,1}(1:end-4) '_cell_beat.jpg'];
    saveas(h30,name,'jpg');
```

```
    % Obtain amplitude spectra
    % First determine a frequency array
    freq = 0:1/(max(time)-min(time)):(length(time)-1)/(max(time)-min(time));

    % We want to calculate and show the amplitude spectrum for sinusoids.
    TF_smooth = abs(fft(beat_xcorr_smooth))*2./length(beat_xcorr_smooth);
    TF_smooth=TF_smooth(1+(0:floor(length(beat_xcorr_smooth)/2)));
    TF_smooth(1)=TF_smooth(1)/2; % freq 0 is special

    % This is repeated for the other signals (smooth, uncorrected and previous
    % frame correction)
    TF = abs(fft(beat))*2./length(beat);
    TF=TF(1+(0:floor(length(beat)/2)));
    TF(1)=TF(1)/2; % freq 0 is special

    TF_uncorrected = abs(fft(beat_uncorrected))*2./length(beat_uncorrected);
    TF_uncorrected=TF_uncorrected(1+(0:floor(length(beat_uncorrected)/2)));
    TF_uncorrected(1)=TF_uncorrected(1)/2; % freq 0 is special

    TF_prev_fr = abs(fft(var_prev_fr))*2./length(var_prev_fr);
    TF_prev_fr=TF_prev_fr(1+(0:floor(length(var_prev_fr)/2)));
    TF_prev_fr(1)=TF_prev_fr(1)/2; % freq 0 is special

    % Only show the first half of the frequency spectrum
    freq(length(TF_smooth)+1:end) = [];
    % Display the frequency spectra
    h40 = figure(40);
    if UStime~=0
        plot([PRF PRF],[0 0.006],'LineStyle', ':', 'LineWidth', 2)
        hold all
    end
    plot(freq,TF);
    hold all
    plot(freq,TF_smooth);
    plot(freq,TF_uncorrected);
    plot(freq,TF_prev_fr);
    hold off
    title([fi{1,1}(1:end-4)])

    xlabel('Frequency (Hz)');
    ylabel('Amplitude (a.u.)');
    grid on
    if UStime~=0
        legend('PRF','xcorr corrected','xcorr smooth corrected','uncorrected','with
regards to prev frame');
    else
        legend('xcorr corrected','xcorr smooth corrected','uncorrected','with regards
to prev frame');
    end
    ylim([0 0.003])

    % Save the frequency spectra
    name = [paresult '\' fi{1,1}(1:end-4) '_cell_beat_freq_content.fig'];
    saveas(h40,name,'fig');
    name = [paresult '\' fi{1,1}(1:end-4) '_cell_beat_freq_content.eps'];
    saveas(h40,name,'epsc');
    name = [paresult '\' fi{1,1}(1:end-4) '_cell_beat_freq_content.jpg'];
    saveas(h40,name,'jpg');

    % Save the results
    name = [paresult '\' fi{1,1}(1:end-4) '_cell_beat.mat'];
    save(name); % In parallel computing (faster, with use of 'parfor'
```

```
    %     %  instead of 'for') save can not be done!
    %     % SAVE is necessary if you want to do ROI analysis so replace 'parfor'
    %     % for 'for' then
end
```

IMPORTFILE_XIMEA.M

```
function EB1control = importfile_ximea(filename, startRow, endRow)
%IMPORTFILE Import numeric data from a text file as a matrix.
%   EB1CONTROL = IMPORTFILE(FILENAME) Reads data from text file FILENAME
%   for the default selection.
%   EB1CONTROL = IMPORTFILE(FILENAME, STARTROW, ENDROW) Reads data from
%   rows STARTROW through ENDROW of text file FILENAME.
% Example:
%   EB1control = importfile('290819 EB 1 control.xiseq', 1, 704);
%    See also TEXTSCAN.
% Auto-generated by MATLAB on 2019/08/30 21:42:17
%% Initialize variables.
delimiter = ' ';
if nargin<=2
    startRow = 1;
    endRow = inf;
end

%% Read columns of data as text:
% For more information, see the TEXTSCAN documentation.
formatSpec = '%q%q%q%q%q%q%q%[^\n\r]';

%% Open the text file.
fileID = fopen(filename,'r');

%% Read columns of data according to the format.
% This call is based on the structure of the file used to generate this
% code. If an error occurs for a different file, try regenerating the code
% from the Import Tool.
dataArray = textscan(fileID, formatSpec, endRow(1)-startRow(1)+1, 'Delimiter',
delimiter, 'MultipleDelimsAsOne', true, 'TextType', 'string', 'HeaderLines',
startRow(1)-1, 'ReturnOnError', false, 'EndOfLine', '\r\n');
for block=2:length(startRow)
    frewind(fileID);
    dataArrayBlock = textscan(fileID, formatSpec, endRow(block)-startRow(block)+1,
'Delimiter', delimiter, 'MultipleDelimsAsOne', true, 'TextType', 'string',
'HeaderLines', startRow(block)-1, 'ReturnOnError', false, 'EndOfLine', '\r\n');
    for col=1:length(dataArray)
        dataArray{col} = [dataArray{col};dataArrayBlock{col}];
    end
end

%% Close the text file.
fclose(fileID);

%% Convert the contents of columns containing numeric text to numbers.
% Replace non-numeric text with NaN.
raw = repmat({''},length(dataArray{1}),length(dataArray)-1);
for col=1:length(dataArray)-1
    raw(1:length(dataArray{col}),col) = mat2cell(dataArray{col},
ones(length(dataArray{col}), 1));
end
numericData = NaN(size(dataArray{1},1),size(dataArray,2));
for col=[5,6]
    % Converts text in the input cell array to numbers. Replaced non-numeric
    % text with NaN.
```

```
    rawData = dataArray{col};
    for row=1:size(rawData, 1)
        % Create a regular expression to detect and remove non-numeric prefixes and
        % suffixes.
        regexstr = '(?<prefix>.*?)(?<numbers>([-]*(\d+[\,]*)+[\.]{0,1}\d*[eEdD]{0,1}[-
+]*\d*[i]{0,1})|([-]*(\d+[\,]*)*[\.]{1,1}\d+[eEdD]{0,1}[-
+]*\d*[i]{0,1}))(?<suffix>.*)';
        try
            result = regexp(rawData(row), regexstr, 'names');
            numbers = result.numbers;

            % Detected commas in non-thousand locations.
            invalidThousandsSeparator = false;
            if numbers.contains(',')
                thousandsRegExp = '^[-/+]*\d+?(\,\d{3})*\.{0,1}\d*$';
                if isempty(regexp(numbers, thousandsRegExp, 'once'))
                    numbers = NaN;
                    invalidThousandsSeparator = true;
                end
            end
            % Convert numeric text to numbers.
            if ~invalidThousandsSeparator
                numbers = textscan(char(strrep(numbers, ',', '')), '%f');
                numericData(row, col) = numbers{1};
                raw{row, col} = numbers{1};
            end
        catch
            raw{row, col} = rawData{row};
        end
    end
end
%% Split data into numeric and string columns.
rawNumericColumns = raw(:, [5,6]);
rawStringColumns = string(raw(:, [1,2,3,4]));
%% Replace non-numeric cells with NaN
R = cellfun(@(x) ~isnumeric(x) && ~islogical(x),rawNumericColumns); % Find non-numeric
cells
rawNumericColumns(R) = {NaN}; % Replace non-numeric cells
%% Create output variable
EB1control = raw;
```

SMOTH_DATA.M

```
function [fitresult, gof] = smoth_data(x, y1)
%CREATEFIT(X,Y1)
%  Create a fit.
%
%  Data for 'untitled fit 1' fit:
%      X Input : x
%      Y Output: y1
%  Output:
%      fitresult : a fit object representing the fit.
%      gof : structure with goodness-of fit info.
%
%  See also FIT, CFIT, SFIT.

%  Auto-generated by MATLAB on 31-Aug-2019 00:12:05
%% Fit: 'untitled fit 1'.
[xData, yData] = prepareCurveData( x, y1 );
% Set up fittype and options.
ft = fittype( 'smoothingspline' );
opts = fitoptions( 'Method', 'SmoothingSpline' );
```

```
opts.SmoothingParam = 0.5;

% Fit model to data.
[fitresult, gof] = fit( xData, yData, ft, opts );

% % Plot fit with data.
% figure( 'Name', 'untitled fit 1' );
% h = plot( fitresult, xData, yData );
% legend( h, 'y1 vs. x', 'untitled fit 1', 'Location', 'NorthEast' );
% % Label axes
% xlabel x
% ylabel y1
% grid on
```

Appendix B – Tested US parameters

Total amounts of repeats performed of every tested set of US parameters.

0.5 MHz	
Pulse duration (ms)	Total measurements (of n samples)
0.7	3(2)
1.0	2(2)
1.4	1(1)
2.0	1(1)

0.7 MHz	
Pulse duration (ms)	Total measurements (of n samples)
0,5	3(2)
0,7	3(2)
1	4(2)

1 MHz	
Pulse duration (ms)	Total measurements (from n samples)
0,001	5(3)
0,002	5(3)
0,005	3(3)
0,01	3(3)
0,02	3(3)
0,05	3(3)
0,1	3(3)
0,2	3(3)
0,3	2(2)
0,4	2(2)
0,5	11(9)
0,7	11(9)
1	23(14)
1,2	1(1)

1.5 MHz	
Pulse duration (ms)	Total measurements (from n samples)
0,002	5(2)
0,004	4(2)
0,008	4(2)
0,02	4(2)
0,04	4(2)
0,1	4(2)
0,2	5(2)
0,3	2(2)
0,5	11(6)
0,7	12(8)
1	7(4)
1,2	7(4)
1,4	1(1)